# Experimental and theoretical studies on mutarotation in supercooled liquid state

Patryk Włodarczyk

Institute of Physics, Uniwersytecka 4, 40-008 Katowice, Poland

University of Silesia

A thesis submitted for the degree of

*PhilosophiæDoctor (PhD), DPhil,..*

2012 05

Supervisor: Prof. Marian Paluch

# Abstract

Carbohydrates are a vast group of biomolecules, which are crucial for biochemical, life processes. As their chemistry and physics have been subject of extensive research, understanding their molecular dynamics in supercooled and glassy region is far from perfect. In a liquid state, many carbohydrates undergo chemical reactions classified as tautomerizations, which are the source of their structural diversity. In the present dissertation mechanism of mutarotation in few monosaccharides, i.e. D-fructose, D-ribose and L-sorbose was investigated. In order to study the mechanism and pathways of mutarotation in supercooled liquid state, the results obtained from dielectric spectroscopy and results obtained from calculations (density functional theory) were compared. The dipole moment analysis performed for D-fructose and D-ribose was used to determine direction of transformations observed by means of dielectric spectroscopy. It was concluded that the last stage of consecutive reactions, i.e. formation of the most stable tautomer (pyranose) from the chain, after quenching of a melt, is monitored. For the D-fructose and D-ribose, the most stable is $\beta$-pyranose form, while for L-sorbose the most stable is $\alpha$-pyranose. The mechanism of mutarotation in supercooled liquid state

was studied by comparing activation energies obtained from dielectric spectroscopy and calculations. The calculations were made for internal and external proton transfer scenarios in the L-sorbose and D-fructose. It was found, that experimentally determined activation energy is higher than that calculated for external proton transfer, but much lower than the energy calculated for internal proton transfer. The unimolecular internal proton transfer as well as bimolecular external proton transfer may occur simultaneously in a supercooled liquid sample. Moreover, analysis of structural relaxation times and rate of mutarotation in the D-fructose leads to the conclusion external proton transfer in the glassy state should be suppressed. In the present thesis experimental methods other than dielectric spectroscopy proved to be useful in the kinetics studies. The rate constants derived from refractive index measurements differ slightly from those obtained by means of dielectric measurements. An impact of mutarotation on the hydrogen bonds structure in monosaccharides has been demonstrated by monitoring changes in secondary mode dynamics in dielectric spectrum. The change of relaxation time or dielectric strength during mutarotation has been shown for all monosaccharides under investigation. It has been concluded that the change of dielectric strength and relaxation time of the secondary mode may vary depending on the type of saccharide.

I dedicate my dissertation work to my family and friends. A special feeling of gratitude to my loving wife, Agnes whose words of encouragement and push for tenacity help in finalizing the thesis. I also dedicate this dissertation to my friends from University of Silesia and Institute of Non-Ferrous Metals who have supported me throughout the process. I will always appreciate all they have done, especially PhD K. Kamiński for helping me develop my technology skills and M.Sc. Eng. J. Szynowski for the many hours of proofreading.

FNP
Fundacja na rzecz Nauki Polskiej

# Acknowledgements

I would like to acknowledge my supervisors: Prof. M. Paluch and Prof. J. Zioło and my co-workers: PhD K. Kamiński, M. Sc. Ż. Wojnarowska and M. Sc. K. Adrjanowicz for stimulating discussions about nature of molecular dynamics of supercooled carbohydrates.

I am also deeply thankful for the financial support of my research within the framework of the project entitled "From Study of Molecular Dynamics in Amorphous Medicines at Ambient and Elevated Pressure to Novel Applications in Pharmacy", which is operated within the Foundation for Polish Science Team Programme cofinanced by the EU European Regional Development Fund.

INNOWACYJNA GOSPODARKA
NARODOWA STRATEGIA SPÓJNOŚCI

UNIA EUROPEJSKA
EUROPEJSKI FUNDUSZ
ROZWOJU REGIONALNEGO

# Contents

# List of Figures

# List of Tables

# 1

# Introduction

## 1.1 Carbohydrates

Carbohydrates (saccharides, sugars) (1–22) are polyhydroxyketons and polyhydroxyaldehydes. The name carbohydrates is referenced to the overall formula $C_m(H_2O)_n$, i.e. hydrates of carbons. This formula is not valid for some complex sugars, deoxysaccharides or aminosaccharides.

Sugars are very important and widespread biomolecules. Nearly 80% of dry mass of plants are carbohydrates (mainly polysaccharides). Polysaccharides are polymers of simple monosaccharides. The most popular polysaccharides are cellulose, starch, glycogen, plant gums (arabic, guar, xanthan, etc.), dextrans and pectins, while the most popular disaccharides are sucrose, maltose and lactose. Fructose and glucose are very important monosaccharides. Sugars play many important roles in living organisms. Glucose dissolved in blood is the main source of energy in animals, while ribose and deoxyribose are backbone of genetic molecules (RNA and DNA). Sugars create biologically important compounds with proteins i.e. glycoproteins and with lipids - glycolipids. Glycolipids are important parts

of neural tissue, cell walls and cell membranes. The main tasks of glycoproteins are coding and message passing. The fact, that organisms use widely oligosaccharides for information exchange and accumulation or for the regulation of life processes, is connected with their enormous coding abilities. Oligosaccharides are obtained by merging monosaccharide units. Every monomer has several function groups (mainly -OH), thus the number of possible combinations created by monomers during merging is really impressive. This is the reason why they are able to code large amounts of data. They can code much more information than the peptides built from the same number of subunits (aminoacid rests). Some oligosaccharides on the surface of cell membranes act as recognizers of cells. Surface oligosaccharides have often acidic rests in their structure, therefore they are negatively charged. Repulsive forces protect cells from aggregating. For example, heparin (known anticoagulant sugar) has the highest negative charge density of all biomolecules (23). Many glycoproteins have sialic acid attached to the sugar molecule. Detaching this acidic rest gives a signal to destroy the protein.

Many sugars are only synthetic and haven't been found in nature. Synthetic sugars are obtained by isomerization or chain modification of the most popular sugars such as glucose, fructose or galactose. The most abundant and cheapest sugars are D-glucose, D-fructose, D-galactose, D-xylose, D,L-arabinose.

Sugars are synthetized by plants during the photosynthesis process, thus these molecules store energy acquired from the sun. Sugars are energy source for plants as well as for animals. Carbon dioxide ($CO_2$) and water ($H_2O$) are used to create glucose or fructose during the photosynthesis. From these sugars, other monosaccharides can be formed in the consecutive reactions. Oligosaccharides and polysaccharides such as cellulose or starch are formed in the oligomerization and poly-

merization reactions. About 50% of dry biomass are glucose polymers. Sucrose, the most known disaccharide consisted of glucose and fructose, is very important saccharide in food industry. It is produced from sugarcane (*Saccharum officinarum*) or sugar beets (*Beta sacharrifera*) and it is used widely as a sweetener. Other important sugars in food industry are glucose and fructose. Fructose is the sweetest sugar of all (1.7 times sweeter than sucrose).

As one can see, sugars are biomolecules of great importance, thus recently many studies on these molecules have been performed (24–46). They are synthetized by living organisms from inorganic substances ($CO_2$, $H_2O$) and they are source of food, storage material and building material. Moreover, they form glycolipids with lipids and glycoproteins with proteins, crucial substances for proper functioning of living organisms.

### 1.1.1 Classification of carbohydrates

The simplest polyhydroxyketons and polyhydroxyaldehydes are dihydroxyacetone and glyceric aldehyde (glyceraldehyde), respectively. All sugars originate from these two compounds (ketoses from dihydroxyacetone and aldoses from glyceric aldehyde). Glucose is the most popular aldose, while fructose is the most popular ketose.

Glyceric aldehyde has two enantiomeric forms i.e., D and L according to the Fischer projection, or (R) and (S) according to the absolute configuration rules. Glyceric aldehyde and dihydroxyacetone are trioses, i.e. carbohydrates consisted of three carbon atoms. Sugars with four carbons are tetroses. The next are pentoses (five carbons), hexoses (six carbons) and heptoses (seven carbons). Another

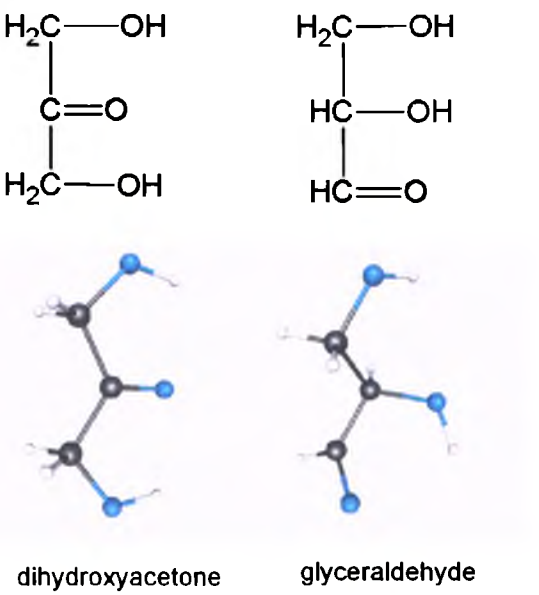


**Figure 1.1:** Trioses - the simplest carbohydrates

classification originates from the ability of sugars to polymerization. Sugars are divided into four groups according to the number of monomers in their structure.

- monosaccharides (1 monomer)
- disaccharides (2 monomers)
- oligosaccharides (few monomers)
- polysaccharides (large number of monomers)

### 1.1.2 Stereochemistry

Sugars that originate from the D-glyceraldehyde belong to the D sugars group. Carbohydrates that originate from L-glyceraldehyde form the L sugar group. Attribution of sugars to the specific group (D or L) is connected with the configuration of the last chiral carbon, i.e. the carbon which is farthest from the

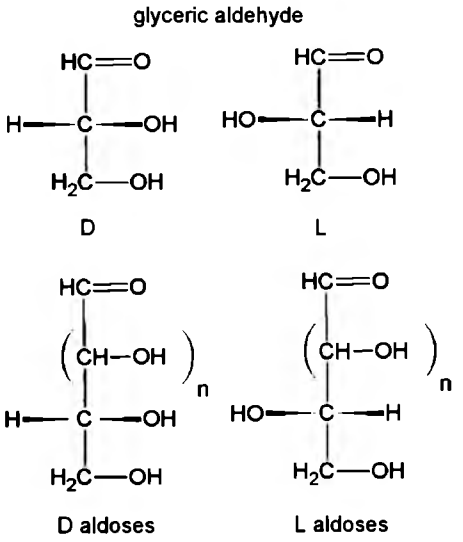


**Figure 1.2:** Fischer projections of D and L-glyceric aldehydes. Rules of classification of aldoses to the D or L group.

carbonyl group. D sugars are more abundant in the nature than the L sugars. Sometimes sugars are marked with small letters *d* or *l*, which is equivalent to (+) and (-). These signs describe specific rotation of sugar, which is not correlated with configuration D or L.

### 1.1.3 Nomenclature

Systematic names of saccharides are complicated, therefore for the majority sugars common names are widely used. Moreover, in the description of olygosaccharides or polysaccharides short three-letter symbols are used (see Table 1.1 for details) Sugars exist mainly in a cyclic form, so in the name of sugar one should find information about ring structure. The name *furanose* is used for ring consisting of five atoms, while *pyranose* is used for the ring consisting of six atoms. Small letters *p* and *f* can be added to the three-letter symbolic name to allow

| common name | symbol |
|---|---|
| glucose | Glc |
| galactose | Gal |
| fucose | Fuc |
| fructose | Fru |
| mannose | Man |
| rhamnose | Rha |
| xylose | Xyl |

**Table 1.1:** Three-letter symbols of most known monosugars.

for mark the type of the ring (p - pyranose, f - furanose). The bond between hydroxyl groups of two different sugars is described by means of an arrow and two numbers, e. g. the notation (1→4) means that the etheric (or glycosidic) bond is formed between the hydroxyl group attached to the C1 carbon in the first sugar and the hydroxyl group attached to the C4 carbon in the second one. Greek letters $\alpha$ and $\beta$ are used to denote the type of anomer. The anomers are two cyclic forms of monosaccharide with the different orientation of the hydroxyl group attached to the so called anomeric carbon atom (it is usually C1 in case of aldose or C2 carbon atom in case of ketose). For example, full systematic name for sucrose is $\alpha$-D-glucopyranosyl-(1→2)-$\beta$-D-fructofuranoside, while its short name is $\alpha$-D-Glc*p*-(1→2)-$\beta$-D-Fru*f*. See Figure 1.3 for better understanding of the nomenclature rules.

### 1.1.4 Monosaccharides - Physical properties

All the aldoses and ketoses families can be obtained from the glyceric aldehyde and dihydroxyacetone, respectively. Full sugar diagrams are presented on Figures

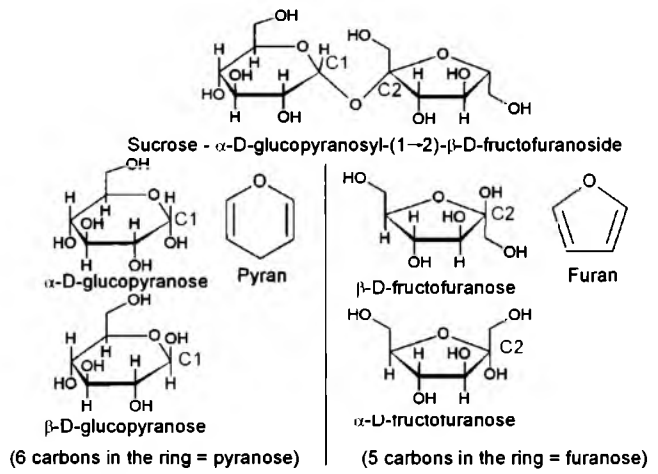


**Figure 1.3:** Structure of sucrose. In the bottom monosaccharide units are presented, both $\alpha$ and $\beta$ anomers. They differ in the position of hydroxyl group by the anomeric carbon atom (C1 and C2, respectively). The name "furanose" originates from furan molecule, while "pyranose" from pyran.

1.4 and 1.5. It is worth noting that these are D sugars, more abundant in nature. Free trioses and tetroses have not been found in the natural environment.

#### 1.1.4.1 Solubility

Glyceric aldehyde, the simplest aldose, is syrup at room temperature. However, it tends to crystallize as dimeric structure. Glyceric aldehyde has good solubility in ethanol and ether and low solubility in water. Dihydroxyacteone also forms dimers and it is easily soluble in water, while hardly in cold ethanol and ether. Erythrose - a syrup at room temperature has great solubility both in water and in ethanol. The pentoses and hexoses (aldoses and ketoses) are crystallic compounds exhibiting good solubility in water and low solubility in methanol and ethanol. They are not soluble in less polar solvents.

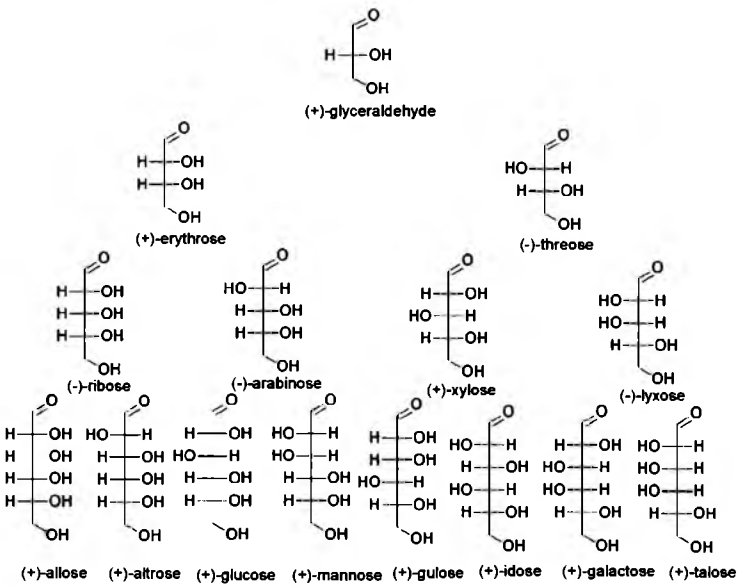


**Figure 1.4:** Family of D-aldoses

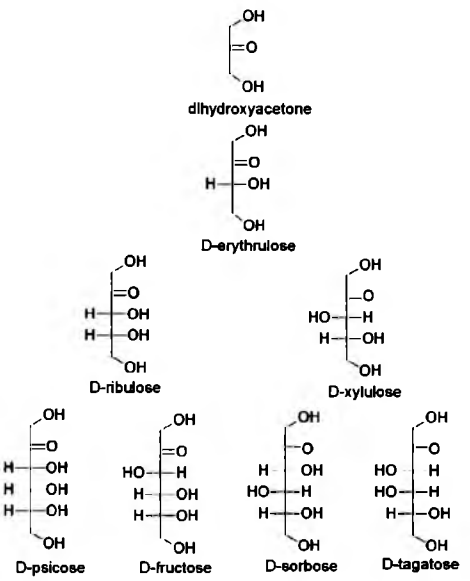


**Figure 1.5:** Family of D-ketoses

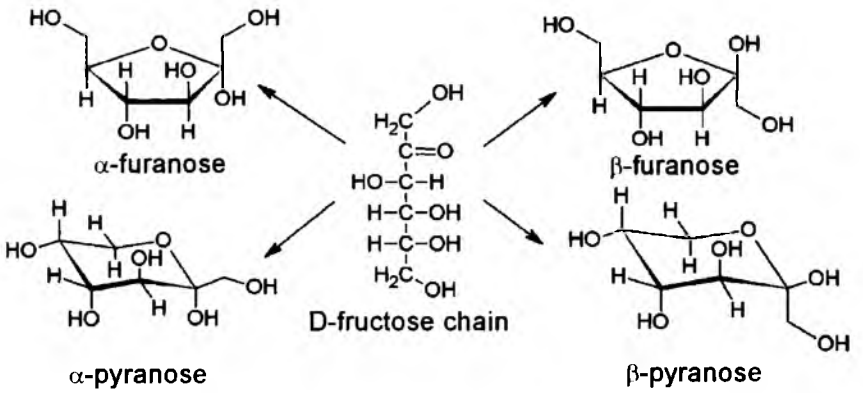


**Figure 1.6:** Hemiacetal forms of D-fructose.

### 1.1.4.2 Mutarotation and anomerization

Aldo- and keto- pentoses and hexoses have a tendency to cyclization and formation of hemiacetalic structure. It is caused by the fact, that in the molecule with carbonyl group and hydroxyl group in the position $\gamma$ or $\delta$, ring can be easily formed in the spontaneous intramolecular cyclization reaction (see Figure 1.6 for details). The hemiacetals formation is connected with the creation of new chiral center, i.e. anomeric carbon atom (C1 for aldoses and C2 for ketoses). The anomeric carbon atom is the most reactive place in the molecule. All aldo- and ketopentoses as well as aldo- and ketohexoses can exist as $\alpha$ and $\beta$ anomers and can attain furanose or pyranose structure due to their tendency of hemiacetals formation. Transformations of rings and anomers are reversible processes, and in solution dynamic equilibrium between these forms is attained. These reactions cause the change in specific rotation of solution $[\alpha_D]$, which is called mutarotation. This phenomenon was discovered over a century ago, in 1846, by Augustin-Pierre Dubrunfaut (47), one of the most famous scientists studying sugars (48). The solution prepared from crystalline $\alpha$-D-glucose has a specific rotation equal to

+112°, but after certain amount of time specific rotation decreases to the value of +52.5°. In a reversed situation, $\beta$-D-glucose dissolved in water has specific rotation of +18.7°, and after the equlibration period, it increases to the same value as in the case of $\alpha$-D-glucose, i.e. +52.5°. Therefore, in both cases the same state is obtained. The phenomenon of anomerization in solution (49–52) can be monitored by various methods, the most popular being polarymetry and NMR (nuclear magnetic resonance). The polarymetry enables direct measurement of specific rotation change. Different anomers/rings can be also distinguished by the $^{1}$H NMR. For example, $\alpha$ anomer of D-glucose has characteristic doublet for H1 at $\delta$=5.12, while similar signal for $\beta$-glucose can be observed at $\delta$=4.53. The $^{13}$C NMR method can be also used for mutarotation studies. Anomeric carbons C1 are distinguishable.

Different tautomers of saccharide (rings or anomers) have different solubility in an aqueous solution and therefore, the least soluble tautomer has priority in the crystallization process. Other tautomers can be crystallized by use of different solvent, like ethanol, acetic acid or pyridine. When the least soluble tautomer starts crystallization, its concentration in a solution decreases and the sample needs to attain new tautomeric equilibrium. In order to attain this new state, transformation of other tautomers to the crystallizing one begins. The whole process is ended when the whole least soluble tautomer crystallize.

Mutarotation can be catalyzed by an acid or a base. In aprotic solvents mutarotation is very slow. Acid accelerates mutarotation by increasing concentration of open chain tautomer. Without the acid or base, mutarotation can occur differently in different environments. In a gas phase mutarotation is a simple proton transfer from the 1OH group to the ring oxygen O. In a liquid phase the situation

is more complicated. There were many studies of this phenomenon in solutions, indicating that mutarotation is very sensitive to the type of solvent. Mutarotation in water, ethanol or pyridine is characterized by different activation energy. In all these cases small solvent molecules are involved in proton transfer, thus the mechanism of this process is intermolecular. there were few studies recently of mutarotation in supercooled liquid and glassy state of pure, anhydrous monosugars (53–58). As there are no low-molecular donors of proton in the system like water molecules, proton could be transfered internally. However, Broido et. al. (59) postulated that in the anhydrous melt other sugar molecules can transfer the proton. There are few papers, in which authors try to explain behavior of mutarotation in the supercooled liquid and glassy states, but the mechanisms of this type of reactions in such viscous phases have not been fully elucidated so far.

Mutarotation can occur also in olygosaccharides. The only condition is to have free hydroxyl group at anomeric carbon. If it is engaged in glycosidic linkage formation, mutarotation is blocked. Two disaccharides, i.e. trehalose and sucrose do not mutarotate due to the specific connection via anomeric hydroxyl groups in both monosaccharide units. These disaccharides are unable to form another glycosidic bonds, so that they are used in mixtures with proteins in order to stabilize them.

#### 1.1.4.3 Purity

Mutarotation and other chemical process - epimerization, i.e. transformation of one saccharide into another isomeric sugar (epimers) in acidic solution - produce a mixture of chemically different tautomers in a sugar sample. The epimers differ in the hydroxyl group placement at C1 or/and C2 carbons. Therefore, there is always

a mixture of tautomers in liquid sugar sample. This fact has many implications. The tendency to crystallization is significantly lowered, thus the sugars can be easily undercooled and many of them exist as syrups.

#### 1.1.4.4 Melting temperature

Anhydrous sugars have relatively high melting temperatures, which is caused by the numerous intermolecular hydrogen bonds created via hydroxyl groups (O-H$\cdots$O). In case of olygo- and polysaccharides, internal hydrogen bonds have significant impact on stabilizing their conformations. For example, in sucrose molecule, there are two, while in celobiose one and in maltose three internal hydrogen bonds. They are formed between two monosaccharide subunits strengthening their connection. Therefore, mobility of monosaccharide units via glycosidic linkage is influenced by internal hydrogen bonds in disaccharides. The internal hydrogen bonds increase their rigidity. Different rigidity is connected with their different physical properties, such as melting point, glass transition temperature, hygroscopic properties, solubility and many others. Some properties of few disaccharides and monosaccharides are listed in Table 1.2.

#### 1.1.4.5 Taste

Mono- as well as di- and olygosaccharides are usually sweet. However, there are some exceptions. The $\beta$-D-mannose is bitter-sweet, while gentiobiose is bitter. Intensity of the sweet taste is characterized by the minimal concentration of sugar, at which the sweet taste can be perceived. A number of monosaccharide units in the sugar influences intensity of a sweet taste. It is caused by the fact that solubility lowers when the number of monosaccharide units increases. Polysaccharides

| Sugar | $T_m$ (K) | $T_g$ (K) | Solubility (g/mL) |
|---|---|---|---|
| Maltose | 433-438 | 360-370 | 1.080 |
| Sucrose | 459 | 340-350 | 2.0 |
| Cellobiose | 512 | 350-380 | 0.12 |
| Glucose | 418-423 | 307 | 0.90 |
| Fructose | 376 | 288 | 4.0 |
| Sorbose | 438 | 293 | 0.55 |
| Ribose | 368 | 263 | >> 4.0 |

**Table 1.2:** Physical properties of mono- and disaccharides. Additional internal hydrogen bonds in disaccharides probably decrease melting temperature and increase solubility (data for room temperature).

are often tasteless due to their low solubility in water. Low molecular sugars differ in quality and intensity of sweetness. The best sweetener is sucrose, which has the nice sweet taste even in high concentration. Fructose is the sweetest of all sugars. It can be sense in water solution with concentration of fructose equal to 0.24%. The next are: glucose (0.8% ), sucrose (1.2% ), maltose (1.4% ) and lactose (2.6% ). Enormous sweetness of fructose is probably caused by high concentration of furanoses in an aqueous solution (60). Sweet taste have also non-sugar substances like polyalcohols (xylitol, sorbitol), aminoacids (glicine, alanine, serine, threonine) and peptides. Dipeptide - aspartame, the sweetener widely used in food industry (especially in fizzy drinks), is about 200 times sweeter than sucrose. However, many authors indicate that aspartame may be dangerous for health as it may be cancerogenic (61).

#### 1.1.4.6 Hygroscopic properties

Crystalline monosaccharides and olygosaccharides can often become liquid because of the high air humidity. Sugars are hygroscopic by nature, and this property is strongly enhanced by the existence of impurities. This is caused by the fact that usually other saccharide impurities disturb the hydrogen bonding structure. Consequently, more hydroxyl groups are free and can absorb water molecules. Saturated solution is then created on the surface of crystal. Absorbed water increases the rate of anomerization processes, which produces even more impurities and increases tendency to forming a liquid. Processes taking place on the crystal surface result in the transportation of molecules from the crystal to the solution on the surface. Consequently, the crystal can be completely liquefied. The least hygroscopic sugars are sucrose, glucose, lactose and maltose. Fructose is more hygroscopic, whereas the mixtures of sugars such as starch syrup or invert sugar (mixture of glucose and fructose) are the most hygroscopic of all.

#### 1.1.4.7 Ring conformations

Carbohydrates form two types of rings i.e. pyranoses and furanoses. Pyranoses can attain chair, skew, boat and half-chair conformations, however energetically favorable pyranoses exist in a chair conformation. There are two stable chair conformations for every monosaccharide, i.e. $^{1}C_{4}$ and $^{4}C_{1}$. The C letter denotes chair conformation, while the superscript denotes atoms above the plane and the subscript denotes the atoms below the plane. The plane is created by the four atoms. In Figure 1.7 $\beta$-fructopyranose is presented in two different conformations. In case of $\beta$-fructopyranose $^{1}C_{4}$ conformation is predominant as more hydroxyl groups exist in equatorial positions. It is a well-known fact that chairs with substituents

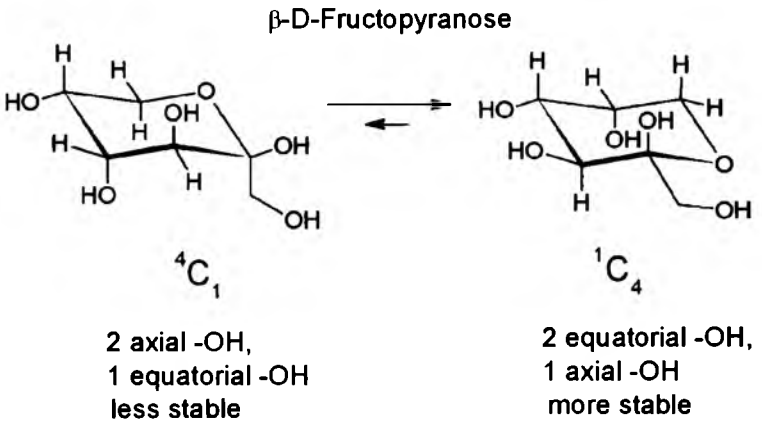


**Figure 1.7:** Two chair conformation of D-Fructose. $^1C_4$ is more stable due to the fact that more of hydroxyl groups is in equatorial positions.

in axial positions exhibit unfavorable 1,3-diaxial interactions. In some cases hydroxyl groups in axial positions are stabilized by hydrogen bonds. Furanoses can exist only in twist or envelope conformation, however they are more diverse and flexible than pyranoses and have similar stability.

#### 1.1.4.8 Supercooled sugars

Monosugars are very good glassformers. Their ability to form glassy state is widely used in food industry. For example, honey is a mixture of supercooled saccharides (mainly fructose and maltose). Many sweets as well as cotton candy are prepared by quenching the melted saccharides. As they are hydrogen bonding systems, their tendency to crystallization should be enhanced due to the ordering feature of hydrogen bonds. However, due to the different chemical reactions that occur during the melting process, crystallization tendency is suppressed by the increase of products concentration. The reactions, such as tautomerization or caramelization (decay at high temperatures) have an impact on melting temperature and

glass transition temperature. Quickly quenched melted saccharides have temperature of glass transition different from that of equilibrated samples (different anomers have different glass transition temperature).

### 1.1.5 Chemical properties

There are many known reactions with sugars. The chain tautomer is mainly involved in the reactions. The most important reactions are: estrification, etherification, oxidation, reduction and sugar transformations such as epimerization. By estrification reaction acetylic saccharides can be obtained. Heating a mixture of sugar and acetic anhydride leads to the peracytelsugars, which are important in food chemistry. For example, octaacetylsucrose is used as quinine substitute due to its bitter taste. Some of the acetic compounds of sucrose are used as emulgators. The most important etheric products of sugar reactions are glycosides. Glycosides are obtained by heating mixtures of sugars and alcohols in the presence of an acid. Alcohol reacts with the hydroxyl group at anomeric carbon as it is the most reactive hydroxyl group. If the sugar is heated with aminoacid N-glicosydes are formed. This process may occur during baking and the products have pleasant smell and taste. In a nature, S-glicosydes are also common. S-glycoside sinigrin has been found in horseradish (*Armoracia rusticana*) and in mustard plant (*Sinapsis*). Other natural glycoside, lincomycin, is antibacterial antibiotic. Oxidation of monosaccharides leads to acids, while reduction leads to alditols (polycalcohols).

Sugars can be mutually transformed in the process called epimerization. In a solution, ketoses can be transformed into aldoses and vice versa. The chain form and enolic form are intermediate states. This process needs to be catalyzed

| Sugar | Price of 1 g in USD | |
|---|---|---|
| | D | L |
| Glucose | 0.02 | 40 |
| Fructose | 0.03 | n/a |
| Galactose | 0.10 | 500 |
| Xylose | 0.20 | 4 |
| Arabinose | 0.50 | 0.45 |
| Mannose | 0.45 | 80 |
| Ribose | 0.65 | 110 |
| Allose | 200 | 900 |
| Gulose | 1300 | 1500 |

**Table 1.3:** Prices of 1 g of monosaccharides in USD.

by acids or bases. In the living organisms, the isomerase enzyme is involved in epimerization. As these reactions lead to the mixture of products in equilibrium, they are not as important as reactions which leads to defined products. There are only few abundant monosugars in the nature, and therefore, most of monosaccharides are synthetic and are obtained from the natural ones (fructose, glucose etc.). There is a little knowledge about the possible application of rare sugars as they are expensive. Prices of different monosaccharides have been compared in Table 1.3.

### 1.1.6 Review of the studied monosaccharides

#### 1.1.6.1 D-fructose

D-fructose, i.e. fruit sugar, is one of the most known sugars. It is produced by green plants in the photosynthesis process. It can be found in fruits, root vegeta-

bles, flowers, honey and in mammals' sperm. The highest content of D-fructose is in apples (43% of all carbohydrates), grapes (45% of all carbohydrates), pears (40% of all carbohydrates) and dried figs (36% of all carbohydrates). It is a part of olygo- and polysaccharides such as: sucrose, rafinose or inuline. About 30 molecules of fructose build insuline hormon. In the past, fructose was obtained from insuline. At present, industrial method of preparing fructose is based on enzymatic conversion of D-glucose. Pure fructose is a white crystalline substance and it is one of the most water-soluble sugars (4.0 g/mL). D-fructose can be also dissolved in alcohols like ethanol. In a crystalline state, fructose exists as $\beta$-pyranose tautomer, while in olygo- or polysaccharides it exists mainly as furanose. In a liquid phase there is an equilibrium between tautomers. In water, at room temperature there is 57% of $\beta$-pyranose (mainly $^1C_4$ conformer), 31% of $\beta$-furanose, 9% of $\alpha$-furanose, 3% of $\alpha$-pyranose and only 1% of open form (52). Due to the mutarotation phenomenon its specific rotation changes from -133° to -92°. Melting temperature is equal to 119-122°C. D-fructose is widely used in food industry due to its sweetness index. It is 1.73 times sweeter than the sucrose. Its sweetness is probably connected with high concentration of furanoses. Very popular sweeteners, especially in North America, are the mixtures of glucose and fructose known as high-fructose corn syrups (HFCS) with different amount of fructose (HFCS-42, HFCS-55 and HFCS-90 - number after the HFCS name means the percentage of fructose). The intake of HFCS is recently connected with obesity epidemy in the United States of America [(62–65)].

#### 1.1.6.2 L-sorbose

L-sorbose is a ketose sugar, epimeric with fructose. It can be found in the fruits of mountain-ash (*Sorbus aucuparia*) or in few lichens. It is obtained from the berries of mountain-ash or from sorbitol by fermentation with *Acetobacter suboxydans* and *A. xylinum*. L-sorbose is a intermediate product of L-ascorbic acid synthesis (C vitamin). In a crystalline state it exists as $\alpha$-pyranose. In the solution it forms equilibrium with small amount of furanoses. The $\alpha$-L-Sorbopyranose exists mainly as $^4C_1$ conformer.

#### 1.1.6.3 D-ribose

D-Ribose is a basic element of nucleic acids, thus it is present in every cell, from viruses to mammals. This simple five carbon sugar is not only a backbone of RNA molecules, but also a builder of ATP molecules. ATP (Adenosine Triphosphate) is a compound, which acts as a energy collector. Fructose, sucrose, glucose and many other sugars are used by organisms as fuel. The D-ribose is different. Organism identifies D-ribose after its intake and then uses it in ATP synthesis. Normal, healthy muscle tissue has the capacity to synthetize all the ribose it needs. Tissue which is stressed by overexertion will be fully recovered in a few days. The real problem appears when the muscles are chronically stressed due to disease or certain conditions that affect tissue energy metabolism. Synthesis of ribose can be in these cases too slow. It is caused by the fact that the heart and muscles don't have the efficient metabolic machinery to make ribose. In consequence, one may suffer from chronic pain, soreness and overwhelming fatigue. Clinical and scientific studies have shown that intake of ribose stimulates energy recovery (66). Tullson

et. al. has shown, that D-ribose administration in fatigued muscles increased the rate of energy recovery by 340% to 430%, depending on tested muscles (67).

## 1.2 Foundations of theoretical methods

Theoretical methods adapted in quantum chemistry can be divided into the methods based on wave function and methods based on electron density. In this work the density functional theory (DFT) was used.

### 1.2.1 Density Functional Theory

Hohenberg and Kohn formulated a theorem, that electron density can be used for the molecular system description instead of a wave function (68). Electron density is given by the equation:

$$\rho(\vec{r}) = N \int \ldots \int |\Psi(\vec{x}_1, \vec{x}_2, \ldots, \vec{x}_n)|^2 ds_1 d\vec{x}_2 \ldots d\vec{x}_n \tag{1.1}$$

By integrating a wave function in spin coordinate of all electrons and in space coordinate of all electrons except one, the function of space coordinates of one electron is obtained. Therefore, electron density is a function of only three variables. Contrary to the wave function, electron density is an observable and it can be measured by X-ray diffraction. The second Hohenberg-Kohn theorem states that there is energy functional $E[\rho]$ with a minimum for the ideal system density $\rho_0$. The Second theorem is a base for the variational Kohn-Sham method (68, 69). In Kohn-Sham approach electrons are chargeless, noninteracting particles. The whole system is influenced by an external potential $\hat{v}_0(\vec{r})$, which ensures the

proper electron density, i. e. electron density of a real system. Kohn-Sham equations can be presented in the form:

$$(-\frac{1}{2}\Delta + \hat{v_0})\phi_i = \varepsilon_i\phi_i \tag{1.2}$$

From the Kohn-Sham orbitals $\phi_i$, electron density can be calculated using the following equation:

$$\rho(\vec{r}) = \sum_{i=1}^{N}\sum_{s}|\phi_i(\vec{r}, s)|^2 \tag{1.3}$$

Construction of detailed Kohn-Sham equations with the explicit form of $\hat{v_0}$ begins from the DFT energy expression:

$$E = T_0 + \int v(\vec{r})\rho(\vec{r})d\vec{r} + J[\rho] + E_{XC}[\rho] \tag{1.4}$$

where $T_0$ is the kinetic energy of noninteracting electrons (particles without charge).

$$T_0 = -\frac{1}{2}\sum_{i=1}^{n} < \phi_i|\Delta|\phi_i > \tag{1.5}$$

The next element in the equation 1.4 is responsible for interactions between electrons and an external potential generated by atomic nuclei. The $J[\rho]$ term describes self-interaction of an electronic cloud.

$$J[\rho] = \frac{1}{2}\iint \frac{\rho(\vec{r}_1)\rho(\vec{r}_2)}{|\vec{r}_1 - \vec{r}_2|}d\vec{r}_1 d\vec{r}_2 \tag{1.6}$$

The last term, $(E_{XC}[\rho])$, is the rest of a missing energy and it is called exchange-correlation energy. This is a mixture of Coulomb correlation, exchange energy and kinetic energy. Mathematical expression for $E_{XC}[\rho]$ is unknown, thus some approximations have to be used.

In order to get solution of Kohn-Sham equation, variational method for energy

expression is applied. The detailed Kohn-Sham equation can be written in the form:

$$(-\frac{1}{2}\Delta + [-\sum_{A}^{M}\frac{Z_A}{r_{1A}} + \int \frac{\rho(\vec{r}_2)}{|\vec{r}_1 - \vec{r}_2|}d\vec{r}_2 + v_{XC}(\vec{r}_1)])\phi_i = \varepsilon\phi_i \tag{1.7}$$

Exchange-correlation potential $v_{XC}$ from the equation 1.7 is defined as:

$$v_{XC} \equiv \frac{\delta E_{XC}}{\delta\rho} \tag{1.8}$$

As the exchange-correlation energy is unknown, it has to be described by approximated functionals. Equation 1.7 is solved iteratively. From the set of starting orbitals, density in zero approximation and then the $\hat{v}_0$ operator are calculated. By solving equation 1.7, a new set of orbitals is obtained and the cycle repeats till self-consistence.

The quality of DFT calculations significantly depends on the type of exchange-correlation functional used. J. Perdew has divided functionals into four groups, which he has called Jacob's ladder (70). The reference points for the functional classes are the solutions obtained by Hartree-Fock method (a method based on wave function theory, in which electron correlation energy is missing), and chemical accuracy.

- chemical accuracy (*HEAVEN*)
- hybrid functionals
- meta-GGA (meta-gradient functionals)
- GGA (gradient functionals)
- LDA or LSD (local or local spin density approximation)

- Hartree-Fock method (*EARTH*)

Recently, double hybrid functionals have been developed to properly describe dispersive forces. The double hybrids are mixtures of hybrid functionals and perturbative MP2 corrections (71–75). They should be placed in the ladder between hybrid functionals and chemical accuracy.

In this study, hybrid functionals were used. Construction of hybrid functionals begins from the expression on the exchange-correlation energy.

$$E_{XC} = \int_0^1 E_{ncl}^{\lambda} d\lambda \tag{1.9}$$

$E_{ncl}$ describes non-classic energy (electron-electron interaction), while $\lambda$ is the coupling force parameter. In other words, $\lambda = 0$ is for the system of non-interacting electrons, whereas $\lambda = 1$ describes fully interacting system. Although the function $E_{ncl}(\lambda)$ is unknown, some cases are well defined. For $\lambda = 0$, $E_{ncl}$ is a Hartree-Fock exchange term.

$$E_X^{KS} = \frac{1}{2} \iint \frac{\rho_0(\vec{r}_1) h_X^{KS}(\vec{r}_1; \vec{r}_2)}{r_{12}} d\vec{r}_1 d\vec{r}_2 \tag{1.10}$$

The second case ($\lambda = 1$) accounts for the situation, when the $E_{ncl}$ can be assumed to be equal $E_{XC}$ of any LDA or GGA functional. Assuming that the $E_{ncl}(\lambda)$ function is linear, $E_{XC}$ of hybrid functional could be expressed as follows:

$$E_{XC}^{HH} = \frac{1}{2} E_{XC}^{\lambda=0} + \frac{1}{2} E_{XC}^{\lambda=1} \tag{1.11}$$

This is the simplest hybrid functional called *half-and-half* functional. As one can see, every hybrid functional is built from the Hartree-Fock exchange term and exchange-correlation terms of a simple gradient or LDA functionals.

The most known, widely used hybrid functional is called B3LYP (76–79). This 3-parameter functional can be written in the form:

$$E_{XC}^{B3LYP} = (1-a)E_X^{LSD} + aE_{XC}^{\lambda=0} + bE_X^{B88} + cE_C^{LYP} + (1-c)E_C^{LSD} \qquad (1.12)$$

The $a$ coefficient controls the amount of exchange energy and the $b$ and $c$ coefficients control contribution of exchange-correlation energy of GGA approximations. The values of $a$, $b$ and $c$ were determined by fitting calculations to experimental values such as atomization energy, ionization potential, etc. and are equal to: $a$=0.20, $b$=0.72 and $c$=0.81.

### 1.2.2 Basis sets

In order to get solutions from DFT method realized by Kohn-Sham equations, it s necessary to assume the form of Kohn-Sham orbitals. Thereafter, one can start solving iteratively the Kohn-Sham equations as stated in the previous section. The Kohn-Sham orbitals are molecular orbitals. Molecular orbital can be presented as linear combination of atomic orbitals (centered on atoms). Atomic orbitals are approximated by a set of functions called basis set. Initially, atomic orbitals were Slater orbitals, which corresponded to a set of functions which decayed exponentially with distance from the nuclei. Radial part of the STO (Slater type orbital) orbital is given as:

$$R(r) = Nr^{n-1}e^{-\zeta r} \qquad (1.13)$$

where $N$ is a normalizing constant, $n$ is the natural number that plays the role of principal quantum number,$r$ is the distance between electron and atomic nucleus and $\zeta$ is a constant related to the effective charge of the nucleus. As the integrals

with Slater type orbitals were often hard to compute, Gaussian type orbitals substituted the Slater type ones. Radial part of the GTO (Gaussian type orbital) is given as:

$$R(r) = Nr^{n-1}e^{-\zeta r^2} \tag{1.14}$$

STO can be approximated by linear combination of GTOs. At present, there are hundreds of basis sets composed of GTOs. The smallest of these are minimal basis sets, which are composed of the minimum number of basis functions, i.e. one function on one atomic orbital. The most common minimal basis sets are STO-nG, where $n$ is an integer. The STO-nG basis set is insufficient for quality research as it do not take into account polarization effects. If the highest occupied atomic orbital is for example $p$, unoccupied $d$ orbitals polarize $p$ orbitals. Therefore, more than one function on one orbital is needed to accurately describe orbital polarization effects. Sometimes very important is an addition of so-called diffuse functions. These are very shallow functions, which more accurately represent the "tail" portion of the atomic orbitals, which are distant from the atomic nuclei. These additional basis functions can be important when considering anions and molecular systems with highly electronegative elements.

Very popular are split-valence basis functions. As the valence electrons are mainly involved in the bonding process, valence orbitals should be composed of more than one basis function (each of which can be composed of a fixed linear combination of primitive Gaussian functions). For example, if we take into account a carbon atom with electron configuration $1s^2 2s^2 2p^2$, the $1s$ orbital is composed of one basis function, while $2s$ and $2p$ are composed of more than one basis function in the split-valence basis set. If the valence orbitals are composed of two basis functions, the basis set is called double-$\zeta$ type. If the orbital is composed of three

functions, basist set is called triple-$\zeta$. One has to remember that every function is a linear combination of GTOs. Typical split-valence basis sets are Pople's basis sets (3-21G, 6-31G, 6-311G). The first number in the basis name accounts for the number of GTOs that build inner-shell orbital, i.e. three in 3-21G and six in 6-31G and 6-311G. The amount of numbers after the "-" sign accounts for the type of basis set (two numbers are for double-$\zeta$, while three numbers for triple-$\zeta$). Each number accounts for the amount of GTOs that create one basis function. For example, in the 6-31G basis set there is one inner-shell basis function created by combination of six GTOs, and two valence functions composed of three and one GTOs, respectively. The Pople's basis sets have often additional marks such as "+" before the "G" letter and asterisks "*" after the "G" letter. Pluses denote additional diffuse functions, while the asterisks denote additional polarization functions.

### 1.2.3 Potential energy surface (PES)

An $N$-atomic molecular system can be described by $3N$ coordinates. 6 independent coordinates describe the translation and rotation of the whole system (5 coordinates for linear molecule, 3 coordinates for atoms). The rest of the coordinates define the internal structure of molecules. The simplest diatomic molecules have 1 energy dependent internal coordinate ($3 * 2 - 5 = 1$), i.e. interatomic distance. The diagram, which represents energy vs. interatomic distance in nitrogen molecule ($N_2$), is presented in Figure 1.8. This is typical Morse potential given by the dependence:

$$V(r) = D(1 - e^{-a(r-r_e)})^2 \tag{1.15}$$

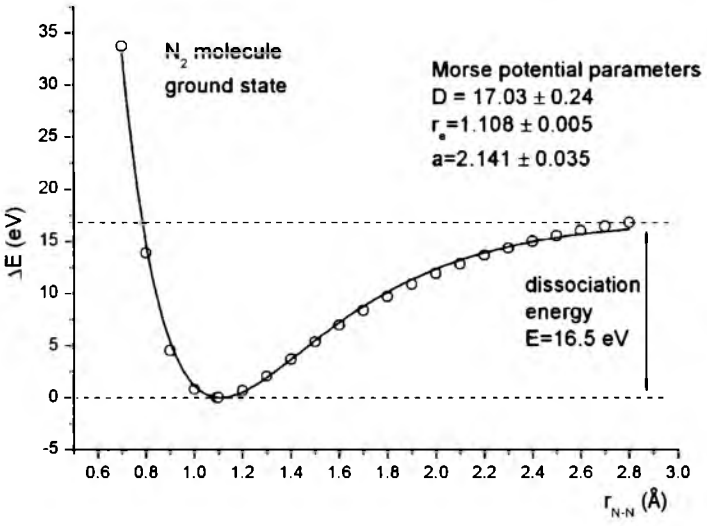


**Figure 1.8:** Diagram of energy as a function of atomic distance in $N_2$ molecule. Energy scan was performed in Orca quantum program on the B3LYP/6-311++G** level of theory. Data was fitted to the Morse curve.

where $D$ is the depth of the potential well, $a$ controls the width of potential, and $r_e$ is an equilibrium bond distance. Energetically most stable structure exists at minimum, whereas the minimum can be reached by changing the N-N distance. Nonlinear molecule composed of 3 atoms (for example water $H_2O$) has $3*3-6=3$ internal coordinates, i.e. 1 angle and 2 bond distances. For 3 coordinates, potential energy forms hypersurface. If one assumes equal O-H bond distances in a stationary state, then only 2 coordinates need to be optimized to obtain energetic minimum (H-O-H angle and O-H distance). The 3D surface plot describing potential energy as a function of angle and bond distance in water is presented in Figure 1.9. More complicated molecules have large amount of internal degrees of freedom, thus they have many minima in the energy surface.

Geometry optimizations performed in quantum mechanics programs are based on simple algorithms with the calculation of first derivatives of energy by the

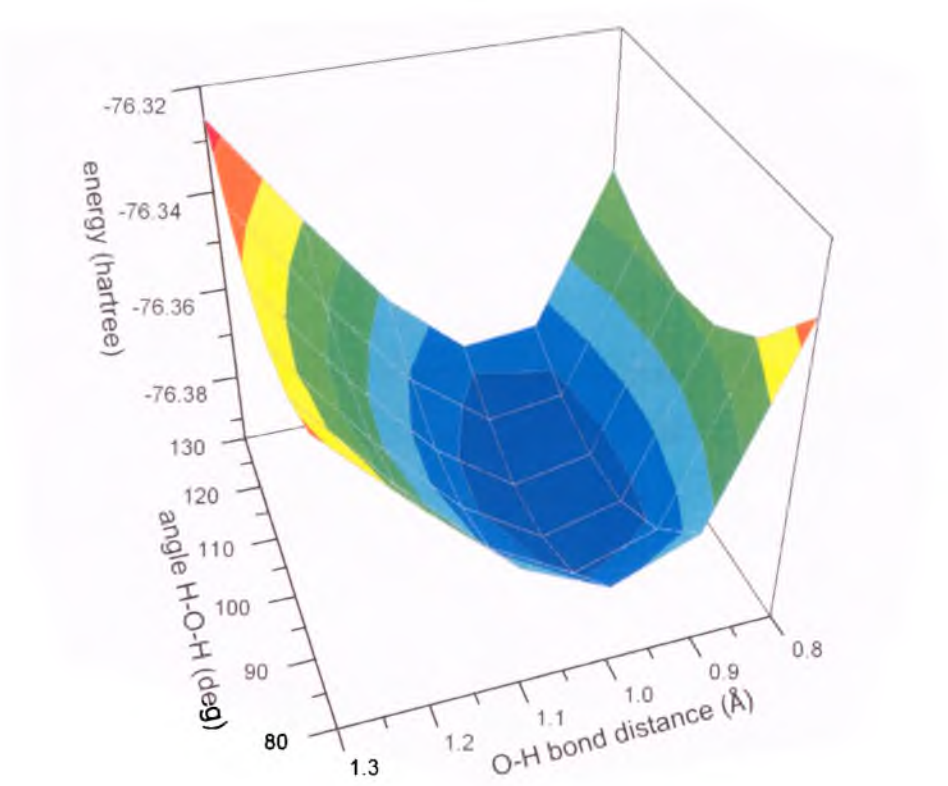


**Figure 1.9:** 3D energy surface of the $H_2O$ molecule. The minimum is clearly visible for the angle of about 105° and bond length of 1 Å.

atoms placement (energy gradients). The energy is calculated iteratively in a single point, then gradients are calculated and the positions of atoms are changed in the direction of decreasing derivative. Therefore, optimization cycles always lead to the nearest local minimum, and in case of complicated molecules it is important to start optimizations from the best possible known geometries. For example, it is known that the most stable conformers of pyranosidic rings of monosaccharides are chairs with the largest possible number of hydroxyl group in equatorial positions.

## 1.3 Chemical kinetics

Chemical kinetics can be defined as analysis of the speed of chemical reactions, their mechanism and influence of different factors on this rate. Although basic laws of chemical kinetics were formulated at the end of XIX century by such scientists as J. H. van't Hoff and S. Arrhenius, formal methods of studying kinetic's mechanism have been developed much later.

### 1.3.1 Speed and order of reaction

The reactions can be divided into homogeneous and heterogeneous ones. Homogeneous reactions occur completely in a single gas or liquid phase, while in heterogeneous reactions substrates can be placed in different phases (reactions of two solids) or in single phase (for example, when gas substrates react on a solid surface). At the constant temperature, speed of a reaction is a function of concentration of reactants, thus it changes continuously during the reaction course.

The speed of reaction is given by the equation:

$$v = \frac{1}{\nu_i} \cdot \frac{dc_i}{dt} \tag{1.16}$$

where $c_i$ is the temporal concentration of the $i$ reactant in moles per volume unit, $t$ denotes time and $\nu_i$ is the stoichiometric coefficient of the $i$ reactant. The speed of reaction can be presented in the form $v = f(c_A, c_b, \ldots, c_l, c_m, \ldots)$ for the reaction described by the equation:

$$aA + bB + \ldots \rightarrow lL + mM + \ldots \tag{1.17}$$

In the simple case, the speed of reaction is a function of concentration of the substrates. Moreover, as the reactant concentrations are the functions of time, the speed of reaction is also a function of time.

Experimental studies have shown that for many reactions, speed of reaction as a function of concentration of reactants has a simple form:

$$v = k \cdot c_a^{\alpha} \cdot c_B^{\beta} \cdot \ldots \tag{1.18}$$

In this kinetic equation, $k$ is the temperature dependent reaction rate constant, while the sum: $x = \alpha + \beta + \ldots$ is the order of reaction. The speed of reaction can be measured by different experimental methods, which allow to monitor concentration of the reactants. As the concentration of a reactant affects different physical properties such as specific rotation, light absorption or conductivity, speed of reaction can be measured by monitoring the changes of physical properties.

### 1.3.2 Fundamental kinetic equations

The order of reaction, which is not related to stoichiometry of reaction, decides about complexity of differential kinetic equation describing the reaction. The

speed of reaction of the first order is given by the equation:

$$v = k \cdot c_A = \frac{1}{\nu_A} \cdot \frac{dc_A}{dt} \tag{1.19}$$

Assuming that at $t = 0$, $c_A = a$ (concentration at the beginning), solution of this differential equation can be presented as follows:

$$\ln \frac{a}{c_A} = kt \tag{1.20}$$

$$c_A = a \cdot \exp(-kt) \tag{1.21}$$

As one can see, concentration of the substrate is decreasing exponentially and the $k$ value is independent on the concentration unit. According to the equation 1.20, the reaction half-life, i.e. the time needed for depletion of half of reactant during the reaction, is equal to:

$$\tau = \frac{\ln 2}{k} \tag{1.22}$$

Unimolecular, as well as bimolecular reactions with the excess of one of the substrates are of the first order.

In the most general case, when the reaction is of the $n$-th order, the reaction rate constant and half-life of reaction are given as follows:

$$k = \frac{1}{(n-1)t} \cdot \left[\frac{1}{c^{(n-1)}} - \frac{1}{a^{(n-1)}}\right] \tag{1.23}$$

$$\tau = \frac{2^{(n-1)} - 1}{(n-1)ka^{(n-1)}} \tag{1.24}$$

### 1.3.3 Kinetics of complex reactions

#### 1.3.3.1 Parallel reactions

The reactions, which can be described by the following diagram, are called parallel reactions.

$$\begin{array}{rcl} & \nearrow & B \\ A & \rightarrow & C \\ & \searrow & D \end{array}$$

There are three independent reaction rate constants ($k_B, k_C, k_D$), which characterize individual reactions. For the first order reactions the following relations are valid. Speed of substrate A depletion is described by the differential equation:

$$-\frac{dc_A}{dt} = (k_B + k_C + k_D)c_A \tag{1.25}$$

which has solution:

$$k_B + k_C + k_D = \frac{1}{t}\ln\frac{a}{c_A} \tag{1.26}$$

$$c_A = a \cdot \exp\left[-\left(k_B + k_C + k_D\right)t\right] \tag{1.27}$$

Temporal concentration of products can be derived from the equation 1.27 and the relation:

$$\frac{dc_B}{dt} : \frac{dc_C}{dt} : \frac{dc_D}{dt} = k_B : k_C : k_D = c_B : c_C : c_D \tag{1.28}$$

#### 1.3.3.2 Consecutive reactions

The consecutive reactions are complex reactions with more than one stage. The simplest consecutive reaction can be described as follows:

$$A \rightarrow B \rightarrow C$$

There is an intermediate $B$ product in the course of the main reaction from $A$ to $C$. The first reaction stage is described by $k_B$, and the second stage by $k_C$. First

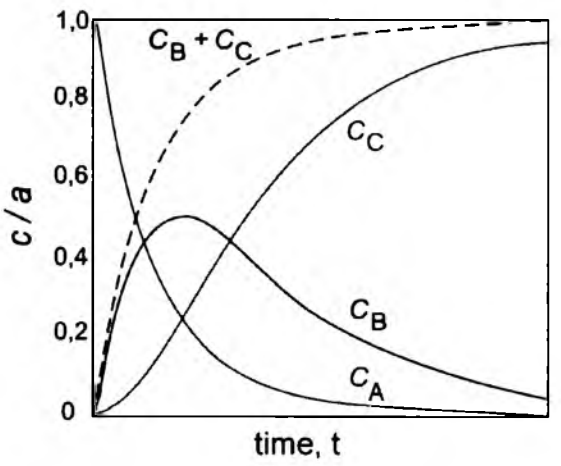


**Figure 1.10:** The diagram illustrating kinetics of elementary reaction in the multistage process.

stage is faster than the second one ($k_B > k_C$). In the Figure 1.10 concentrations of substrate $A$ and products $B$ and $C$ as a function of time are plotted. The concentration of $A$ decreases exponentially in accordance with the equation 1.21. Concentration of $B$ initially rises to a maximal value and then lowers constantly. It is caused by the different reaction speeds of two stages of elementary reactions. The intermediate product $B$ quickly accumulates in the system and then slowly interconverts into final product ($C$). Concentrations of the products $B$ and $C$ are given by the functions:

$$c_B = \frac{k_B \cdot a}{k_C - k_B} \cdot \left(e^{-k_B t} - e^{-k_C t}\right) \tag{1.29}$$

$$c_C = a - ae^{-k_B t} - \frac{k_B \cdot a}{k_C - k_B} \cdot \left(e^{-k_B t} - e^{-k_C t}\right) \tag{1.30}$$

where $a$ is the concentration $c_A$ at the beginning of reaction (t=0).

#### 1.3.3.3 Reversible reactions

Reversible reaction can be expressed as follows:

$$A \rightleftharpoons B$$

The forward reaction is described by the rate constant $k$, while the reverse reaction is described by the rate constant $k'$. At the beginning of the reaction there is only $A$ substrate with the concentration $a$. During the reaction, product $B$ is formed with the concentration $x$. When the equilibrium is achieved, $x$ approaches the $x_e$ value. The equation for reversible reaction can be written in the form:

$$x = x_e\{1 - exp[-(k + k')t]\} \tag{1.31}$$

### 1.3.4 Temperature dependence of a rate constant

The speed of chemical reaction usually significantly depends on temperature. Basing on earlier works by J. H. van't Hoff, S. Arrhenius formulated his equation describing the relation between rate constant $k$ and temperature $T$.

$$\frac{d\ln k}{dT} = \frac{E}{RT^2} \tag{1.32}$$

Integration of this equation leads to the expression:

$$k = A\exp\left[-E/(RT)\right] \tag{1.33}$$

where $R$ is the activation energy. Activation energy of the majority of reactions is equal to the value between 50 and 300 kJ/mol. Activation energy is approximately temperature independent.

### 1.3.5 Transition state theory

Transition State Theory was formulated by Marcus and Rice (80, 81), H. Eyring and co-workers (82–84), Magee (85), Rabinovitch and co-workers (86), and later by Bunker and co-workers (87–90).

Reactants and products are placed in energetic minima, and so-called transition state (activated complex) is a structure on the route between reactants and products. In the simplest substitution reaction given by the equation:

$$X + YZ \rightarrow XY + Z$$

The energy continuously rises as the X atom approaches the YZ molecule . At a certain distance, the energy achieves a maximum value characteristic for the transition state. From that point, energy decreases as X atom approaches Y and Z atom strays away. In this theory the energy is changing continuously and the reaction proceeds via the intermediate structure called the transition state.

As the molecules are usually complex with many internal degrees of freedom, reactions pathways are located on the energy hyper-surfaces. In that case, transition state has maximum of energy only in one dimension (in the internal reaction coordinate). It has a minimum of energy for the rest of internal coordinates. Such point in multidimensional surface is called the 1st order saddle point. In three dimensions it looks like a ravine in the mountains (see Figure 1.11 for details).

#### 1.3.5.1 Determination of the 1st order saddle point by QM methods

In order to calculate energy barrier of reaction, geometry of the 1st order saddle point needs to be optimized. The most popular algorithm is the eigenvector

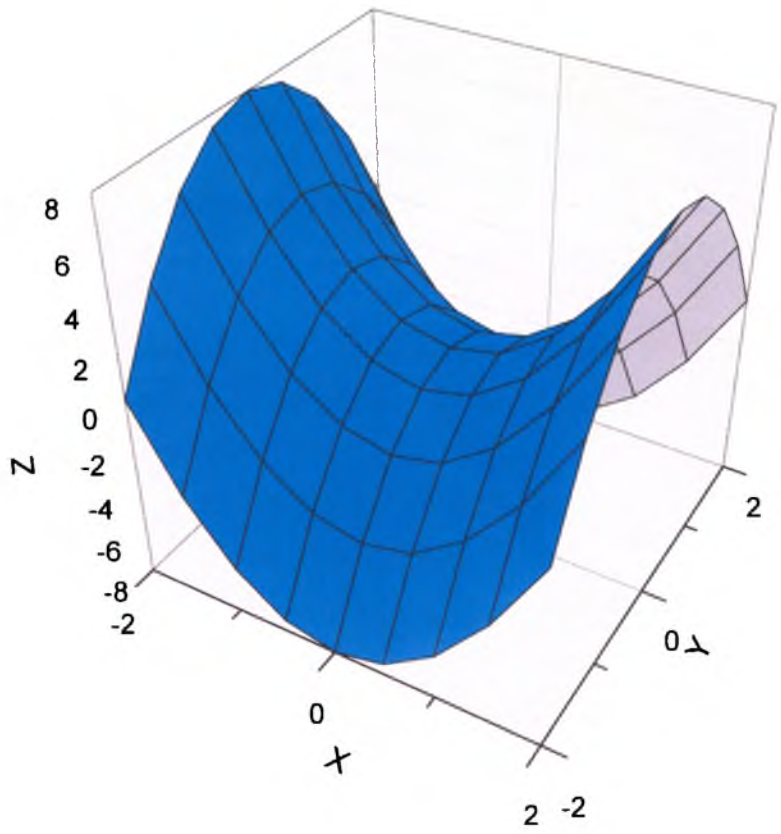


**Figure 1.11:** 1st order saddle point in the 3-dimensional surface. Surface is described by the function $z = 2 \cdot (x^2 - y^2)$. Saddle point is located at coordinates S=(0,0,0).

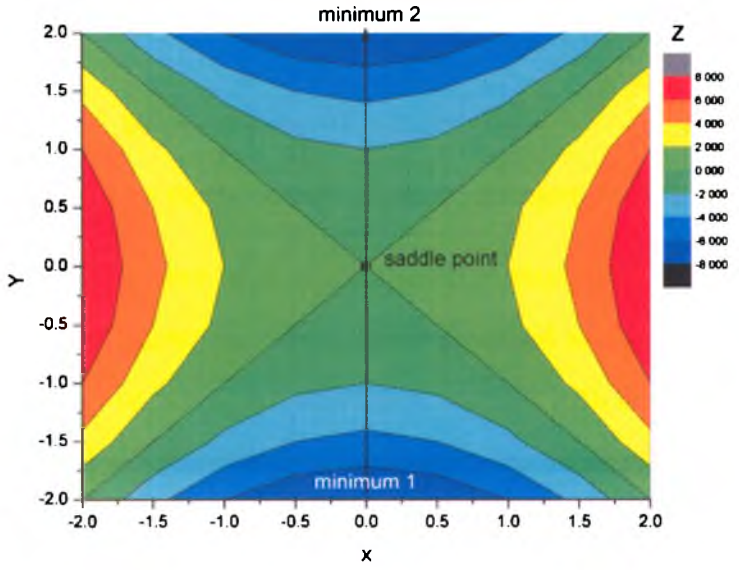


**Figure 1.12:** The saddle point on 3-dimensional surface in 2D contour representation. The arrow shows the route of hypothetical reaction.

following method. In order to optimize stationary state, the Hessian has to be calculated (matrix of second derivatives of energy by the atom placement). The Hessian calculated for molecule which is located in a saddle point on energy surface has one negative eigenvalue. Optimization algorithm is similar to the standard geometry optimization which leads to a minimum. The geometry changes during optimization so that energy achieves maximum in one direction and a minimum value in the rest of directions. Geometry optimization must be started from the point which is close to the searched structure. Such close geometry is obtained from relaxed geometry scans.

# 1.4 Foundations of dielectric spectroscopy

## 1.4.1 Electric properties of molecules

### 1.4.1.1 Microscopic properties – dipole moment & polarizability

Dielectric material has very weak electric conductivity. Substances with specific electrical resistivity higher than $10^7\Omega\cdot$ m are classified as dielectrics. These substances can be polar or non-polar, which is connected with the dipole moment of their molecules. Dipole moment for a system of point charges is defined as:

$$\vec{\mu} = \sum_i q_i \vec{r_i} \tag{1.34}$$

The SI unit of the dipole moment is C · m, however more popular is debye unit (1 D= $3.33564 \cdot 10^{-30} C \cdot m$). When the electric dipole is placed in the electric field, torque is induced:

$$\vec{\tau} = \vec{\mu} \times \vec{E} \tag{1.35}$$

This torque causes that the dipoles try to orientate along the electric field direction.

There are 3 types of electric dipoles:

- Permanent dipoles – their atoms have different electronegativity and they have low symmetry. These electric dipoles exist without the external electric field
- Temporal dipoles – formed due to the dynamic heterogenities in the electron cloud distribution
- Induced dipoles – formed in the external electric field. They vanish in the absence of an electric field

Molecules are built of positively charged nuclei and negatively charged electron cloud. External electric field disturbs the equilibrium between charges by shifting them. In a consequence, even in the molecule without the permanent dipole moment, electric field is able to create induced dipole moment $\mu_i$. For weak electric fields, induced dipole moment depends linearly on the strength of electric field.

$$\vec{\mu_i} = \alpha \cdot \vec{E_l} \tag{1.36}$$

In this equation, $E_l$ is a local electric field, while $\alpha$ denotes polarizability. Polarizability is the symmetric tensor of the second order with 6 independent values. This equation can be written in a matrix form:

$$\begin{pmatrix} \mu_{x,i} \\ \mu_{y,i} \\ \mu_{z,i} \end{pmatrix} = \begin{pmatrix} \alpha_{xx} & \alpha_{xy} & \alpha_{xz} \\ \alpha_{yx} & \alpha_{yy} & \alpha_{yz} \\ \alpha_{zx} & \alpha_{zy} & \alpha_{zz} \end{pmatrix} \begin{pmatrix} E_{x,l} \\ E_{y,l} \\ E_{z,l} \end{pmatrix} \tag{1.37}$$

Dipole moment is a vector, thus it depends on the structure of the molecule. If the molecule is highly symmetric, the sum of vectors is equal to 0, and permanent dipole moment $\mu = 0$. For example, $CCl_4$ (Td symmetry), benzene (D6h symmetry) or borane $BH_3$ (D3h) have $\mu = 0$, thus these molecules are non-polar. If the symmetry of molecule is lower, it becomes polar. For example, water with C2v symmetric point group has a dipole moment equal to $\mu = 1.85$ D. The value of dipole moment is related to the electronegativity of molecule's elements. Huge differences in electronegativity cause large shifts of the electron cloud, which in consequence enhances differences in atomic charges. For example, as fluorine (F) is more electronegative than chlorine (Cl), from two linear molecules HF and HCl, the former one has higher dipole moment. The dipole moment of HF is in fact equal to $\mu = 1.9$ D, while the dipole moment of HCl is equal to $\mu = 1.1$ D.

#### 1.4.1.2 Macroscopic properties – polarization

The parallel-plate capacitor with the charges $+q$ and $-q$ on its plates has the capacitance in the vacuum equal to $C_0$. Strength of the electric field between plates is equal to $E_0$. When the dielectric material is placed between the plates its capacitance rises to the value of C.

$$C = \varepsilon C_0 \tag{1.38}$$

$\varepsilon$ is the dimensionless, temperature dependent dielectric permittivity which is characteristic for dielectric material. While the capacitance with dielectric material is higher, electric field strength between plates is lower.

$$\vec{E} = \frac{\vec{E_0}}{\varepsilon} \tag{1.39}$$

This is caused by the polarization effects in the capacitor. The molecules of dielectric polar material in a constant electric field try to orientate in accordance with the electric field direction. Ordering of the electric dipoles causes polarization of dielectric material, which is known as orientational polarization. As the orientational polarization is temperature dependent, high temperature causes ordering suppression.

Electric field acts on dielectric material (polar and non-polar) causing deformational polarization. Deformational polarization is caused by shifting positive and negative charges in the molecules resulting in inducing weak dipole moments. This effect occurs independently of orientational polarization.

In order to study these phenomena, three vectors should be defined at this point. The dielectric shift vector $\vec{D}$ is related to the external electric field strength

$\vec{E}$ by the equation:

$$\vec{D} = \varepsilon_0 \varepsilon \vec{E} \tag{1.40}$$

The polarization vector $\vec{P}$ is defined by two equations:

$$\vec{D} = \varepsilon \vec{E} + \vec{P} \tag{1.41}$$

$$\vec{P} = \varepsilon_0 \chi^{(1)} \vec{E} \tag{1.42}$$

where $\chi^{(1)}$ is linear suscebility, $\varepsilon_0$ is vacuum permittivity and $\varepsilon$ is dielectric permittivity. Equations 1.36 and 1.42 describe the same phenomenon on the microscopic and macroscopic level, respectively. The $\chi^{(1)}$ and $\varepsilon$ are symmetric tensors of the second order.

For the case of non-polar dielectric material, dielectric polarization vector is given by the formula:

$$\vec{P} = N\mu_i = \frac{1}{V} \sum_{j=1}^{N} \mu_{i,j} \tag{1.43}$$

where N is the number of induced dipoles per unit volume. Effective electric field strength is related with polarization vector:

$$\vec{E_{ef}} = \frac{\vec{P}}{\varepsilon_0 (\varepsilon - 1)} \tag{1.44}$$

Effective electric field is the field inside the dielectric material, not an external electric field. Effective electric field can be approximated by various models. In the Lorentz model the molecule is placed into empty sphere inside the polarized dielectric material. The radius of the sphere is much greater than the molecule radius. Effective electric field strength is equal to:

$$\vec{E_{ef}} = \vec{E} = \frac{1}{3\varepsilon_0} \vec{P} \tag{1.45}$$

The Clausius-Mossotti equation for molar polarization of non-polar dielectric material has been derived basing on the Lorentz model:

$$\Pi_{ind} = \frac{\varepsilon - 1}{\varepsilon + 2}\frac{M}{\rho} = \frac{N_0}{3\varepsilon_0}\alpha \qquad [m^3 \cdot mol^{-1}] \tag{1.46}$$

This equation connects macroscopic properties with microscopic ones. However it is based on the approximation of an effective field.

While the deformational polarization is practically temperature independent, orientational polarization decreases with increasing temperature, which is caused by the chaotic thermal molecular activity. The theory of temperature dependence of orientational polarization was developed by P. Debye. It is based on the Langevin theory for paramagnetic substances.

The potential energy of interaction between electric dipole and effective electric field is given by the formula:

$$V = -\vec{\mu} \cdot \vec{E_{ef}} = \mu E \cos(\theta) \tag{1.47}$$

As one can see, the minimum of energy corresponds to the situation when the dipole is oriented in parallel to the electric field ($\theta = 0$). However, thermal fluctuations cause that in dielectric sample dipoles are oriented at different angles. For a fairly low temperatures (near room temperature) and in low electric fields (less than $10^4$ V/m), the average value of dipole moment projection on the field direction is given by the relation:

$$\bar{\mu} = \frac{\mu^2 E_{ef}}{3kT} \tag{1.48}$$

Taking this into account, Debye has derived an equation for molar polarization of polar molecules:

$$\Pi = \Pi_{ind} + \Pi_{or} = \frac{\varepsilon - 1}{\varepsilon + 2}\frac{M}{\rho} = \frac{N_0}{3\varepsilon_0}\left(\alpha + \frac{\mu^2}{3kT}\right) \tag{1.49}$$

#### 1.4.1.3 Dielectric material in changing electric field

In order to study polarization behavior in a changing electric field, polarization behavior after sudden turning an electric field on and off needs to be considered. After turning the electric field on, deformational polarization achieves maximum value almost instantly. The deformational polarization can be expressed as follows:

$$P_{\infty} = \varepsilon_0(\varepsilon_{\infty} - 1)E \tag{1.50}$$

where $\varepsilon_0$ is permittivity of a vacuum and $\varepsilon_{\infty}$ is the permittivity when electric field frequency achieves infinity (from Maxwell relation it is equal to the square of refractive index $\varepsilon_{\infty} = n^2$). Orientational polarization rises much slower and achieves maximum value after a certain period of time. Orientational polarization can be expressed as follows:

$$P_{or} = \varepsilon_0(\varepsilon_s - \varepsilon_{\infty})E \tag{1.51}$$

where $\varepsilon_s$ is static permittivity (permittivity, when frequency of the electric field achieves 0). After turning off the electric field deformational polarization drops very fast, whereas orientational polarization vanishes slowly. Rising and vanishing of orientational polarization after turning electric field on and off is known as dielectric relaxation. Polarization changes in time are described by relaxation function $\Phi(t)$ which is of exponential character.

$$\Phi(t) \sim \exp\left(\frac{-t}{\tau_D}\right) \tag{1.52}$$

where $\tau_D$ is dielectric relaxation time and characterizes dynamic properties of molecules of dielectric material. Relaxation function describes response to a disturbance caused by an external electric field. If the electric field frequency is high

enough, it is too fast for dielectric material polarization. Process of molecules reorientation needs certain period of time so as to overcome resistance of the system (e.g. viscosity). Therefore, there is a phase shift between $\vec{P}$ and $\vec{E}$, as well as between $\vec{D}$ and $\vec{E}$. In a non-static case, dielectric permittivity is a complex function, which can be defined as:

$$\varepsilon^* = \frac{D_0}{\varepsilon_0 E_0} e^{-i\delta} \tag{1.53}$$

where $\delta$ is a phase difference between $\vec{D}$ and $\vec{E}$. This phase difference depends on field frequency $\omega$, thus $\varepsilon^*$ is a function of $\omega$.

$$\varepsilon^*(\omega) = \varepsilon'(\omega) - i\varepsilon''(\omega) \tag{1.54}$$

The real part of dielectric permittivity is given as:

$$\varepsilon'(\omega) = \frac{D_0}{\varepsilon_0 E_0} \cos\delta(\omega) \tag{1.55}$$

while imaginary part of dielectric permittivity is given as:

$$\varepsilon''(\omega) = \frac{D_0}{\varepsilon_0 E_0} \sin\delta(\omega) \tag{1.56}$$

In the static case, $\omega$=0 which implies that $\delta$=0. Consequently, $\varepsilon'' = 0$, while $\varepsilon' = \varepsilon_s$ In the limit $\omega \to \infty$, $\varepsilon'' = 0$ and $\varepsilon' = \varepsilon_\infty$.

The Debye-Pellet relaxation model is the simplest model describing the phenomenon of dielectric relaxation. It can be written in the form:

$$\frac{\varepsilon^* - \varepsilon_\infty}{\varepsilon_s - \varepsilon_\infty} = \frac{1}{1 + i\omega\tau_D} \tag{1.57}$$

The real part of this equation can be written as:

$$\frac{\varepsilon' - \varepsilon_\infty}{\varepsilon_s - \varepsilon_\infty} = \frac{1}{1 + (\omega\tau_D)^2} \tag{1.58}$$

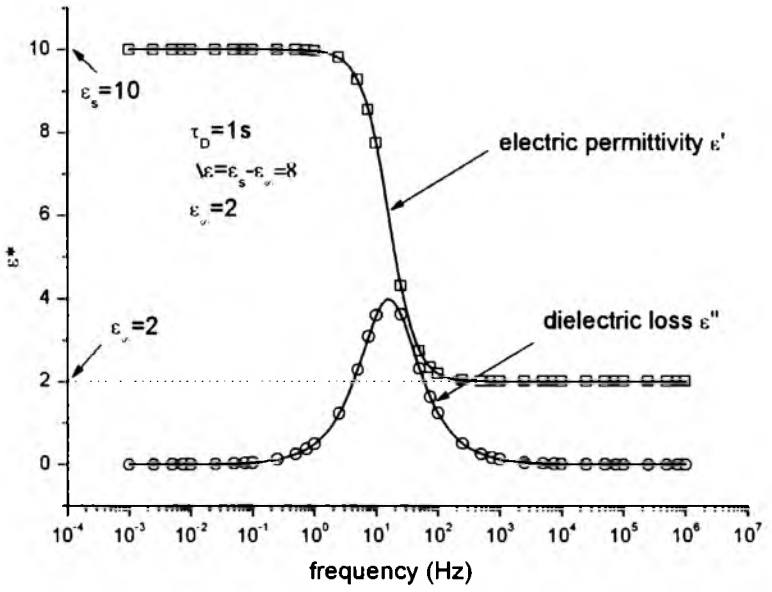


**Figure 1.13:** Hypothetical dielectric spectrum described by the Debye-Pellet model.

while the imaginary part is equal to:

$$\frac{\varepsilon''}{\varepsilon_s - \varepsilon_\infty} = \frac{\omega\tau_D}{1 + (\omega\tau_D)^2} \tag{1.59}$$

Typical diagram of dispersion $\varepsilon'(\omega)$ and dielectric absorption $\varepsilon''(\omega)$ is presented in Figure 1.13. Dielectric loss curve reaches a maximum at relaxation time $\tau_{max}$ which is the most important dynamic parameter. In the dielectric spectrum curves have usually non-Debye shapes, which is caused by the distribution of relaxation times, hydrogen bonds or other phenomena taking place in the sample. Havriliak-Negami model is the most universal model which can describe majority of dielectric spectra with different shapes. It is empirical modification of the Debye-Pellet model.

$$\frac{\varepsilon^* - \varepsilon_\infty}{\varepsilon_s - \varepsilon_\infty} = \frac{1}{(1 + ((i\omega\tau_D)^\alpha)^\beta)} \tag{1.60}$$

where the parameters $\alpha$ and $\beta$ describe assymetry and broadness of the peaks. They are changing from 0 to 1.

#### 1.4.1.4 Molecular dynamics and dielectric spectra

Dielectric spectroscopy is a great method for studying dynamics of glass-forming liquids. There are few relaxation processes in the spectrum of such sample. The slowest relaxation process is related to the cooperative motion of liquid molecules and it is called structural relaxation. This process has strong, non-Arrhenius temperature dependence of relaxation times. It is related to the viscosity of the system as it is a factor which hinders orientation of dipoles in the electric field. Structural relaxation governs glass transition phenomenon. Faster relaxation processes are known as secondary modes, which are coupled to more local movements of molecules. Secondary mode can be related to the rotation of entire molecules as well as to the conformational activity of molecule. Secondary modes exhibit the Arrhenius behavior of relaxation time vs. temperature.

# 2

# The objectives of dissertation

## 2.1 Main objective

Although mutarotation was discovered more than a century ago, studies on this process in supercooled liquid phase were presented for the first time in a few papers that I have published since 2009 and which are the basis for this PhD thesis (53–56). The first publication was inspired by two works by Tombari et. al. (91, 92) who have discovered thermal hysteresis of $C_p$ during calorimetric measurements of $\beta$-D-fructose, which was caused by mutarotation. Moreover, the work by Fan et. al. (93) indicated that viscosity of a system may change during mutarotation. Mutarotation was earlier reported for a glassy state of lactose in the work by Lefort et. al. (94). After publication of my work, several other papers were published on mutarotation in supercooled liquid and in a glassy state (57, 95).

The main objective of this work was to study the kinetics and elucidate the mechanism of mutarotation in simple monosaccharides in supercooled liquid phase and to indicate some differences between this reaction in supercooled

liquid and glassy state.

## 2.2 Specific objectives

Several specific scientific targets have been accomplished on the way. The studies of mutarotation in different types of saccharides lead to understanding of the role of hydrogen bonds in this process. The changes in hydrogen bonds pattern are related to the fast secondary mode in monosaccharides. Therefore, behavior of secondary mode relaxation during mutarotation has been investigated. In order to explain the mechanism of mutarotation in supercooled liquid phase, DFT calculations were carried out to check differences in activation energy for the mechanisms based on internal proton transfer as well as on external proton transfer in L-sorbose and D-fructose. By comparative analysis of dipole moments in D-fructose and D-ribose, possible pathways of mutarotation in quenched melted monosaccharides have been discovered. At last, the changes in specific volume and refractive index of saccharide D-fructose during mutarotation have been also investigated.

# 3

# Discussion

## 3.1 Experimental results

### 3.1.1 Dielectric spectroscopy

Typical dielectric spectrum of monosaccharide is presented in Figure 3.1. Two processes can be easily identified. At higher temperatures structural $\alpha$-relaxation is clearly visible, while at low temperatures, in the glassy state, secondary $\gamma$-relaxation can be observed. Studies on the molecular dynamics of monosaccharides have been recently performed by Kaminski et. al. (96). The authors have shown, that there is a hidden $\beta$-relaxation process behind the structural relaxation peak. Therefore, clearly visible secondary mode is labeled in the literature as $\gamma$. This $\gamma$ mode has been identified by the same authors as the dynamic movement of hydroxymethyl unit (-$CH_2OH$ group) (97). In this chapter, an impact of mutarotation on molecular dynamics will be explained. Moreover, kinetics of mutarotation in supercooled liquid state will be evaluated based on the changes of parameters of molecular dynamics.

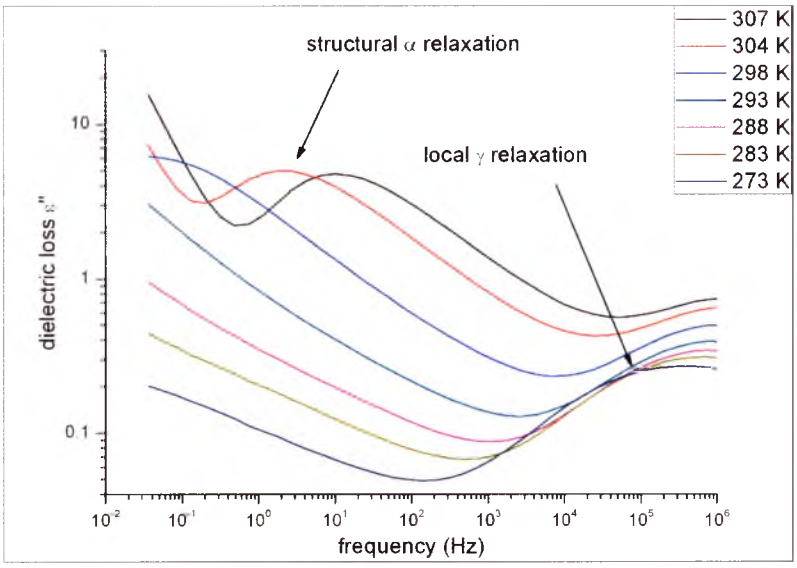


**Figure 3.1:** Dielectric spectrum for D-fructose equilibrated at 298 K.

#### 3.1.1.1 Structural relaxation

The structural relaxation process can be influenced by mutarotation phenomenon. It has been observed, that structural relaxation characteristic time may change at constant temperature in saccharides which tend to form furanoses in a liquid state (e.g. fructose or sorbose), if the sample is unequilibrated. If one quenches melted sugar to a certain temperature, the sample will be temporarily out of equilibrium. The whole equilibration process could be observed by monitoring structural relaxation behavior at isothermal conditions. Shifting of structural relaxation of D-fructose is presented in Figure 3.2. Structural relaxation is connected to the viscosity of a liquid. The more viscous is the studied sample, the longer structural relaxation time. In case of D-fructose, D-ribose and L-sorbose structural relaxation peak of unequilibrated sample at a constant temperature is shifting towards lower frequencies. It means that the relaxation time becomes longer, and the liq-

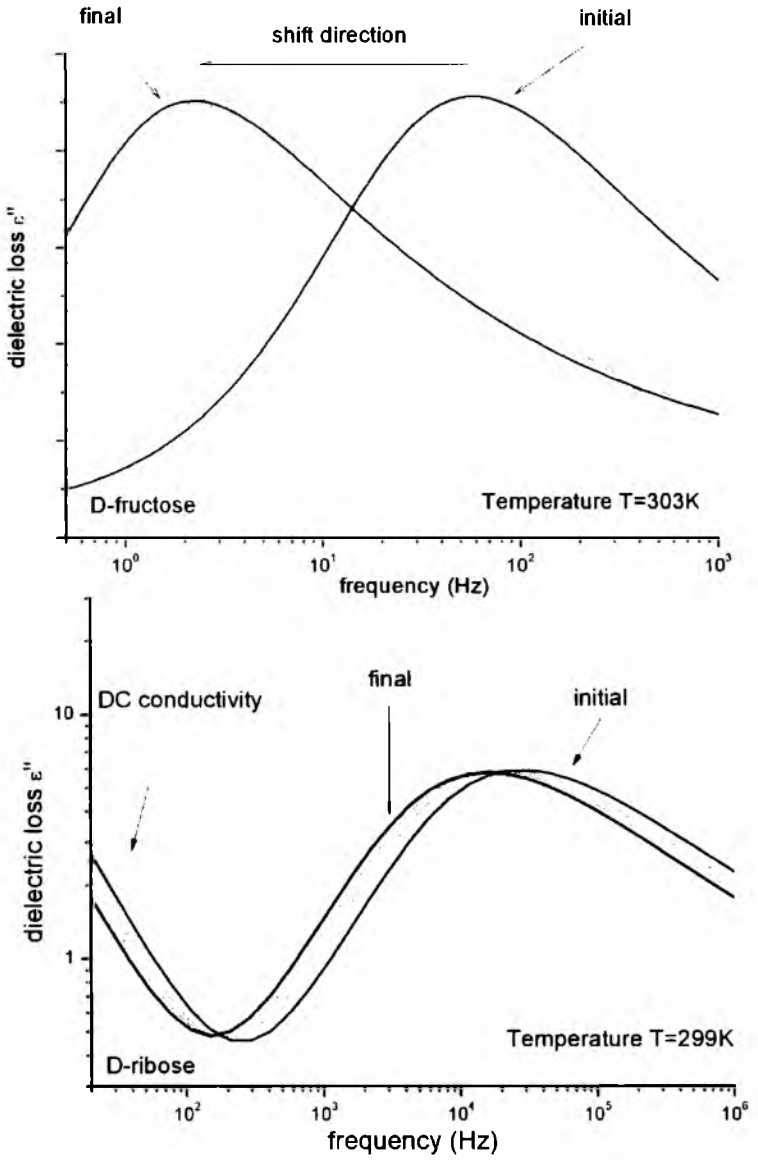


**Figure 3.2:** Shift of structural relaxation during isothermal equilibration.

| Sugar | $T_g$ of uneq. sample (K) | $T_g$ of eq. sample (K) | $\Delta T_g$ |
|---|---|---|---|
| L-sorbose | 291 | 296 | 5 |
| D-fructose | 282 | 293 | 11 |
| D-ribose | 256 | 262 | 6 |

**Table 3.1:** Glass transition temperatures of equilibrated and unequilibrated studied saccharides. The strongest effect is observed in D-fructose

uid becomes more viscous during the process of mutarotation. As the structural relaxation is related to the viscosity and it governs glass transition, it affects also glass transition temperature. As the dynamics slows down, the glass transition temperature becomes higher. The differences in glass transition temperatures between freshly quenched and equilibrated samples are presented in Table 3.1. Glass transition temperature was obtained as a temperature at which relaxation time is equal to $\tau = 100$ s.

#### 3.1.1.2 Constructing kinetic curves

Displacement of structural relaxation peak can be used to derive kinetic parameters of mutarotation. The rate of shifting structural relaxation in time at isothermal conditions is connected to the change of particular tautomer concentration. Therefore, kinetic curves are obtained by plotting structural relaxation time vs. time. For every temperature, shift has been observed within different frequency ranges. In order to compare these curves on a single diagram, kinetic curves can be scaled as follows:

$$\alpha_D = \frac{\tau - \tau_p}{\tau_k - \tau_p} \tag{3.1}$$

| L-sorbose | | D-fructose | | D-ribose | |
|---|---|---|---|---|---|
| T (K) | k ($s^-1$) | T (K) | k ($s^-1$) | T (K) | k ($s^-1$) |
| 313 | $1.58 \times 10^{-4}$ | 313 | $4.57 \times 10^{-5}$ | 296 | $2.37 \times 10^{-5}$ |
| 318 | $2.58 \times 10^{-4}$ | 318 | $1.12 \times 10^{-4}$ | 299 | $3.48 \times 10^{-5}$ |
| 323 | $3.09 \times 10^{-4}$ | 323 | $2.10 \times 10^{-4}$ | 302 | $5.90 \times 10^{-5}$ |
| 328 | $5.36 \times 10^{-4}$ | 328 | $2.66 \times 10^{-4}$ | 305 | $7.83 \times 10^{-5}$ |
| 333 | $7.79 \times 10^{-4}$ | 333 | $5.72 \times 10^{-4}$ | | |
| activation energy $E_a$ (kJ/mol) | | | | | |
| L-sorbose | | D-fructose | | D-ribose | |
| $67.7 \pm 3.9$ | | $107.0 \pm 5.7$ | | $105.1 \pm 6.5$ | |

**Table 3.2:** Rate constants and activation energies for D-fructose, D-ribose and L-sorbose.

where $\alpha_D$ is called degree of reaction, $\tau$ is current relaxation time, $\tau_p$ - relaxation time at the beginning of reaction (relaxation time of the first monitored peak),$\tau_k$ - relaxation time at the end of reaction. Kinetic curves for different sugars and different temperatures are shown in Figures 3.3 and 3.4 The speed of every reaction is characterized by temperature dependent rate constant, and as the mutarotation is the 1-st order reaction, the rate constant $k$ has the dimension $s^{-1}$. Rate constants for L-sorbose, D-fructose and D-ribose have been compared in Table 3.2. As one can see, mutarotation in supercooled liquid phase of D-fructose and D-ribose is similar. It is rather slow and is characterized by similar activation energy (approx. 105 kJ/mol). In sorbose, mutarotation is much faster near room temperature. However, lesser activation energy causes, that its temperature dependence is not such strong as in two other monosaccharides. Very interesting is the kinetic curve of D-fructose at the lowest temperature studied. It

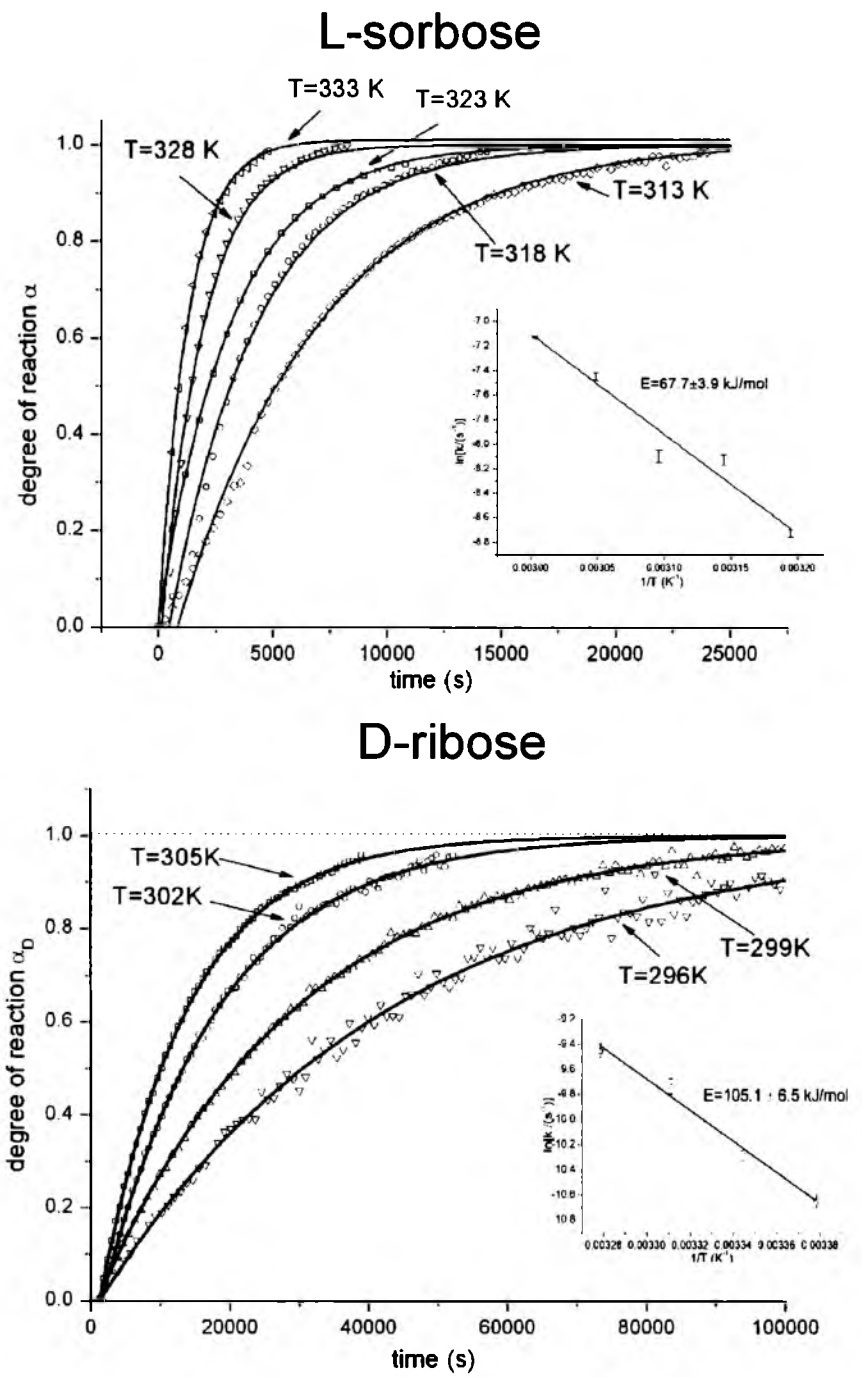


**Figure 3.3:** Kinetic curves for L-sorbose and D-ribose and D-fructose. Activation energy plots are added in the insets

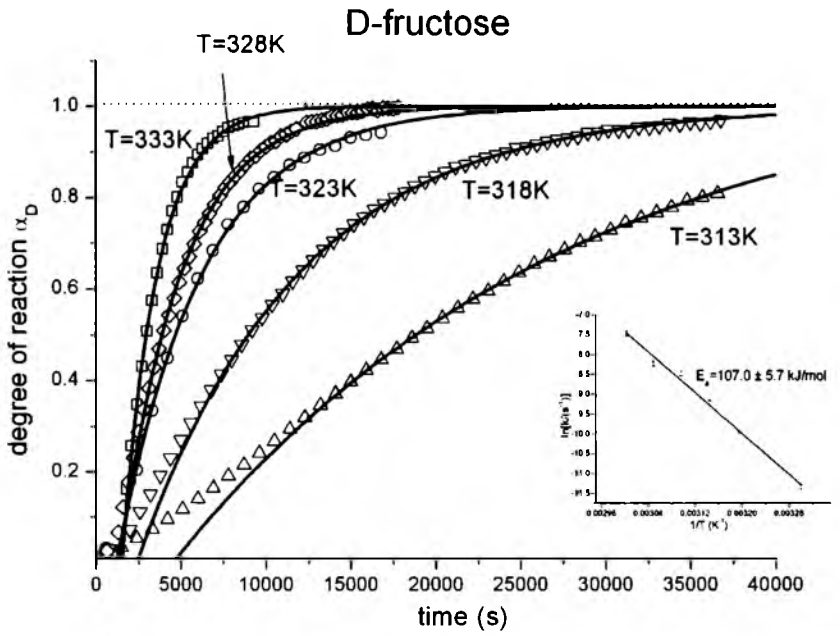


**Figure 3.4:** Kinetic curves for D-fructose. Activation energy plot is located in the inset.

has sigmoidal shape and can be described by exponential function only above the inflection point. Such curve is characteristic for autocatalytic processes, however in such complex environment as in liquid saccharide, this can be accounted for a single stage of consecutive reaction (see curve C in Figure 1.10 for details). It means, that only a single, the latest stage of reaction is monitored by means of dielectric spectroscopy. As the other methods "see" average effect of mutarotation, this may be an advantage of dielectric spectroscopy.

#### 3.1.1.3 Secondary mode

Secondary mode ($\gamma$-relaxation) is related to the local hydroxymethyl ($CH_2OH$) substituent movement. As this group is connected by external hydrogen bonds with other molecules, mutarotation should affect the $\gamma$-process. This relaxation

mode can be clearly seen in the dielectric spectrum at low temperature in the glassy state. In order to check the impact of mutarotation on $\gamma$-relaxation, saccharide sample was quenched to the temperature of about 173 K and measured. Afterwards, the same sample was heated to 303 K, equilibrated for 48 hours, and then cooled down to 173 K and measured again. The differences in $\gamma$-relaxation in studied saccharides are presented in Figure 3.5. Secondary mode change was also observed by Singh et. al. (95) in D-lyxose. Different behavior of this mode has to be connected with the reformation of hydrogen bonds in the system. In case of L-sorbose and D-fructose strength of hydrogen bond network is similar after equilibration period. Contrary to this situation, in D-ribose hydrogen bonds become weaker at the end of mutarotation process. It can be caused by the fact, that D-ribose in pyranosidic form is deprived of hydroxymethyl groups. This was postulated in the reference (97).

#### 3.1.1.4 Static permittivity

Static permittivity, i.e. the value of real part of permittivity at low frequency (dielectric constant), is connected with the permanent dipole moments of the molecules inside dielectric material. As different tautomers can have totally different dipole moments, mutarotation phenomenon should affect average dipole moment and, consequently static permittivity. In the D-ribose and D-fructose static permittivity changes were monitored by means of dielectric spectroscopy. In these two molecules an opposite effect has been observed: dielectric constant of D-ribose drops , whereas dielectric constant of D-fructose rises as the mutarotation begins. This fact will be useful when the reaction paths will be predicted.

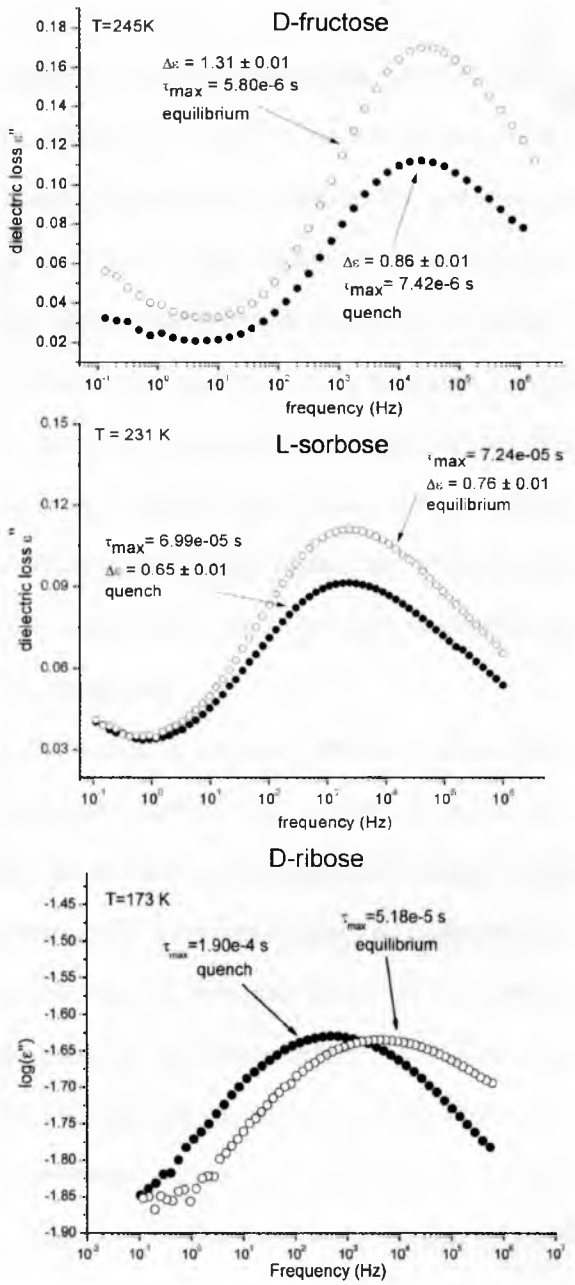


**Figure 3.5:** Impact of mutarotation on $\gamma$-relaxation. In case of D-fructose and L-sorbose dielectric strength improvement is observed, while in D-ribose relaxation time was changed.

### 3.1.2 Other experimental methods

Mutarotation was always studied in solutions so that usually optical methods were used for kinetic studies. In case of viscous, supercooled liquids these methods became hard to apply. For example, filling the polarimeter tube with melted sugar could be very hard due to the vitrification process occurring in the tube. Some researches use chromatography or NMR for studies (98-100), but these methods are good for studying solutions. Very recently, Raman spectroscopy was successfully used for studying glucose mutarotation in the glassy state (58), while dielectric spectroscopy has become one of the leading methods in the studies of tautomerizations in supercooled liquid phase, not only in sugars (101). However, dielectric spectroscopy seems to be sensitive only to certain stages of the reaction (in which viscosity is changing).

Other experimental methods, such as refractive index measurements and specific volume (PVT) measurements were checked whether they could be successfully used to monitor mutarotation in supercooled liquid phase.

The PVT measurements were conducted in cooperation with Prof. J. Pionteck from Leibniz Institute of Polymer Research Dresden in Germany. Melted D-fructose was quenched to the temperature T=303 K, and then specific volume was measured as a function of time at sightly elevated pressure (10 MPa). Elevated pressure is necessary to hinder the formation of any bubbles due to evaporation of possible moisture or decomposition products which would falsify the measured specific volume data. The plot of specific volume $V_{sp}(cm^3/mol)$ versus temperature $T(K)$ is presented in Figure 3.6. As one can see, resolution of PVT apparatus is sufficient to detect mutarotation phenomenon. The data were fitted

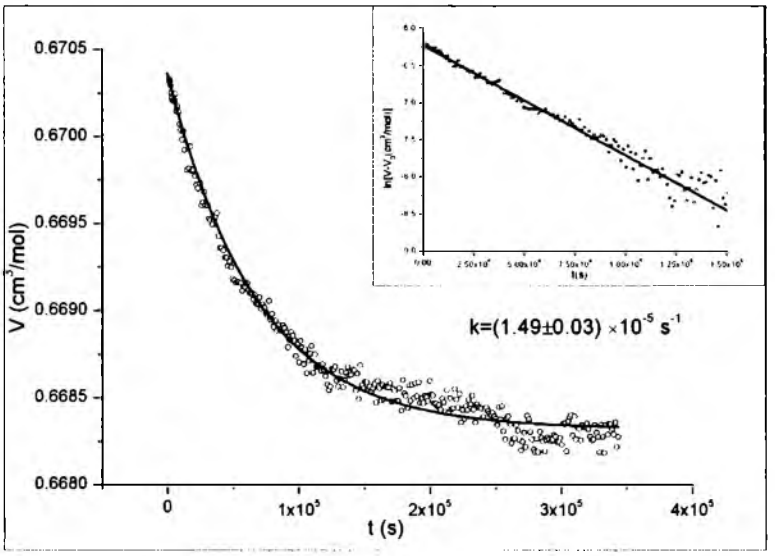


**Figure 3.6:** Specific volume change in time during mutarotation in D-fructose. The data were fitted to the 1st order equation in the exponential and linear form (inset).

to the exponential 1st order equation in the form:

$$V = A \cdot \exp(-kt) + V_0 \tag{3.2}$$

The same equation can be written in the linear form:

$$\ln(V - V_0) = \ln A - kt \tag{3.3}$$

During the mutarotation phenomenon contraction of specific volume is observed. The rate constant of this process at T=303 K and at the pressure p=10 MPa is equal to $1.49 \cdot 10^{-5} s^{-1}$ which is comparable to the rate constant obtained from dielectric spectroscopy, i.e. $1.39 \cdot 10^{-5} s^{-1}$ at the ambient pressure p=0.1 MPa and temperature T=303 K.

In case of refractive index measurements, the rate constants and activation energy were derived. Refractive index of supercooled fructose was measured by

| Temperature (K) | Rate constant [BDS] ($s^{-1}$) | Rate constant [RI] ($s^{-1}$) |
|---|---|---|
| 313 | 4.57 x $10^{-5}$ | 8.78 x $10^{-5}$ |
| 318 | 1.12 x $10^{-4}$ | 1.59 x $10^{-4}$ |
| 323 | 2.10 x $10^{-4}$ | 2.83 x $10^{-4}$ |
| 328 | 2.66 x $10^{-4}$ | 4.94 x $10^{-4}$ |
| 333 | 5.72 x $10^{-4}$ | 8.48 x $10^{-4}$ |
| $E_a$ (kJ/mol) | 107.0 $\pm$ 5.7 | 98.3 $\pm$ 3.5 |

**Table 3.3:** Comparison of rate constants and activation energies for D-fructose mutarotation obtained from dielectric spectroscopy [BDS] and refractive index measurements [RI].

means of Abbe's refractometer. By plotting refractive index versus time, kinetic curves were constructed. Thereafter, the rate constants and activation energy were obtained. All the obtained data have been summarized in Table 3.3. As one can see, rate constants derived from optical measurements are significantly higher. Moreover, activation energy derived from refractive index measurements is slightly smaller. It can be caused by the fact, that optical measurements monitor an average effect of mutarotation, while dielectric spectroscopy monitors final stage of consecutive reactions.

## 3.2 Theoretical results

The Mechanisms of mutarotation in simple monosaccharides was also studied by means of density functional theory (DFT) method. Analysis of dipole moments has been performed in D-ribose and D-fructose, while calculations of energy barriers have been performed in D-fructose and L-sorbose. Internal and external proton transfers have been checked in the latter saccharides. All the calculations were

| D-ribose | | D-fructose | |
|---|---|---|---|
| tautomer | dipole moment (D) | tautomer | dipole moment (D) |
| $\beta$-D-pyranose | 2.15 | $\beta$-D-pyranose | 3.54 |
| $\beta$-D-furanose | 2.56 | $\beta$-D-furanose | 0.66 |
| $\alpha$-D-furanose | 3.21 | $\alpha$-D-furanose | 2.94 |

**Table 3.4:** Dipole moments of particular tautomers of D-ribose and D-fructose. Dipole moments of D-ribose are calculated as weighted average from dipole moments of 5 most stable conformers, whereas dipole moments of D-fructose are presented for the one most stable conformer.

started for the optimized structures. Geometry optimizations were performed on a random, hand-modeled structures on the B3LYP/6-31+g(d,p) level of theory.

### 3.2.1 D-fructose

In the D-fructose, non-catalyzed internal proton transfer was checked in three most abundant tautomers, i.e. $\beta$-pyranose, $\alpha$-furanose and $\beta$-furanose. Interconversions in furanoses are quite interesting, as the transition state as well as the minima have internal hydrogen bonds. During the transformation, energy increase caused by the deformation of the ring was partially compensated by the enhancement of hydrogen bond strength. This can be seen in the visualization diagram in Figure 3.7. The calculated activation energies were relatively high. Energy of the formation of $\beta$-fructopyranose is equal to 165 kJ/mol, while energies of decay of $\alpha$- and $\beta$-furanose are equal to 149 and 154 kJ/mol respectively. This is by 50-60 kJ/mol more than the experimentally obtained activation energy. Dipole moment values have been calculated for the most stable tautomers (cyclic minima in Figure 3.7) of D-fructose. The dipole moments are gathered in Table 3.4.

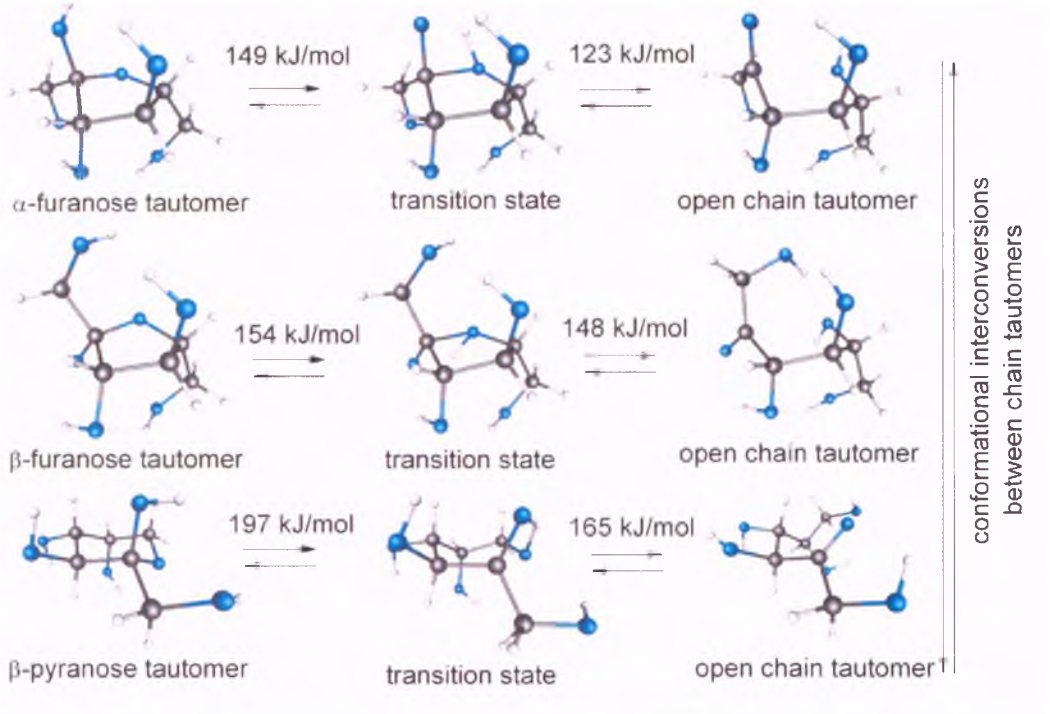


**Figure 3.7:** Visualization of internal proton transfer mechanism in three fructose tautomers.

For the D-fructose, formation of $\beta$-pyranose with an additional water molecule has been checked. Activation energy of this process is equal to 66 kJ/mol.

### 3.2.2 D-ribose

In D-ribose, different tautomers were optimized for further dipole moment determination. Five of the most stable optimized tautomers were used for average dipole moment calculations. The calculated dipole moments are gathered in Table 3.4. The dominant tautomer, i.e. $\beta$-pyranose, has the lowest dipole moment (2.15 D), while less stable furanoses have from 0.5 to 1 D higher dipole moments. This scenario is opposite to that in D-fructose. In D-fructose the most stable tautomer has very high dipole moment (3.5 D), while furanoses have lower dipole moments (0.7-3 D).

### 3.2.3 L-sorbose

All tautomers were optimized for L-sorbose, i.e. $\alpha$-pyranose, $\alpha$-furanose,$\beta$-furanose and $\beta$-pyranose. Three tautomers (without $\beta$-pyranose ) were further optimized with one water molecule and finally, the system with two $\alpha$-pyranoses was also calculated. In the first stage, internal proton transfer from the anomeric hydroxyl group to the ring oxygen in four tautomers was checked. Energy barriers for such conversion are relatively high. However, in case of pyranoses, if the transfer is made from hydroxyl group in equatorial position, the energy is slightly lower than in case of a transfer from hydroxyl group in an axial position. The calculated energies are shown in Table 3.5. For the transformation in a direction from chain to ring, the lowest energy was obtained for $\alpha$-sorbofuranose and $\alpha$-sorbopyranose

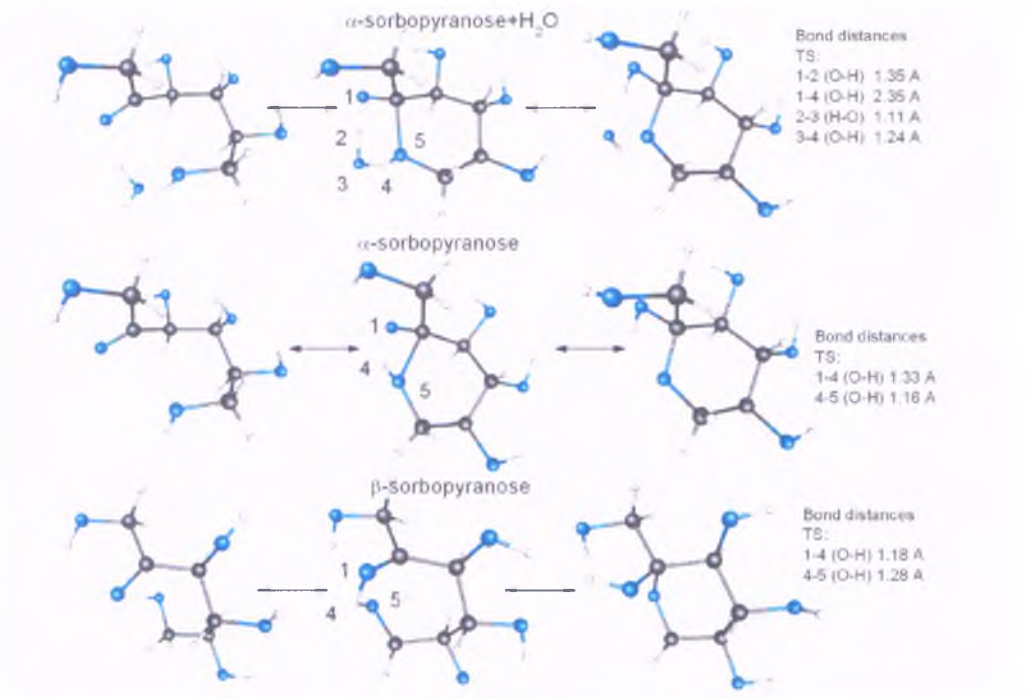


**Figure 3.8:** Visualization of sorbopyranoses mutarotation

(135.7 and 137.9 kJ/mol, respectively). Comparison of energy barriers for transformations in the reverse direction has shown that the lowest energy barrier is for the $\alpha$-sorbofuranose decay (142.8 kJ/mol). At the near room temperatures mainly decay of less stable structures, i.e. furanoses and $\beta$-sorbopyranose, and the formation of most stable structure i.e. $\alpha$-sorbopyranose, should be observed. In comparison to the value obtained experimentally i.e. 68 kJ/mol, energies obtained for internal proton transfer are far too high. Calculations with additional water molecule were performed to check the energy barriers in case of intermolecular mechanism. As one can see, agreement between experimental and theoretical values is in this case very good. Formation of $\alpha$-sorbopyranose has activation energy equal to 75.7 kJ/mol. This value is very close to the one obtained by analysis of data from dielectric spectroscopy. In Figure 3.8 one can compare the

| tautomer | $E_a$ of formation (kJ/mol) | $E_a$ of decay (kJ/mol) |
|---|---|---|
| $\alpha$-sorbopyranose | 137.9 | 158.7 |
| $\beta$-sorbopyranose | 163.3 | 170.3 |
| $\beta$-sorbofuranose | 159.8 | 168.1 |
| $\alpha$-sorbofuranose | 135.7 | 142.8 |
| $\alpha$-sorbofuranose + water | 59.9 | 77.8 |
| $\alpha$-sorbopyranose + water | 75.7 | 86.3 |
| $\beta$-sorbofuranose + water | 76.4 | 92.3 |
| 2 × $\alpha$-sorbopyranoses | 47.8 | 63.2 |
| expt | 68 | |

**Table 3.5:** All the calculated activation energies for L-sorbose transformations (B3LYP/6-31+G(d,p))

tautomerization process in sorbopyranoses with and without water molecule.

### 3.2.4 Double proton exchange in L-sorbose and D-fructose

Monosaccharides are hydrogen-bonding molecules. Therefore, there is a possibility that proton could be exchanged between two monosaccharide molecules. Broido et. al. (59) postulated that such process might occur in melted saccharides. As this is another scenario of intermolecular process, this mechanism was checked by calculations. Energy barrier for the proton exchange in two $\alpha$-sorbopyranoses was obtained. The energies for decay and formation of two molecules at the same time are given in Table 3.5. The decay of pyranoses is related to the energy equal to 63.2 kJ/mol, whereas formation of pyranoses from chain tautomer is connected with energy equal to 47.8 kJ/mol. The whole process has been visualized in Figure 3.9. . Energy barriers are surprisingly low and the value of the decay energy is

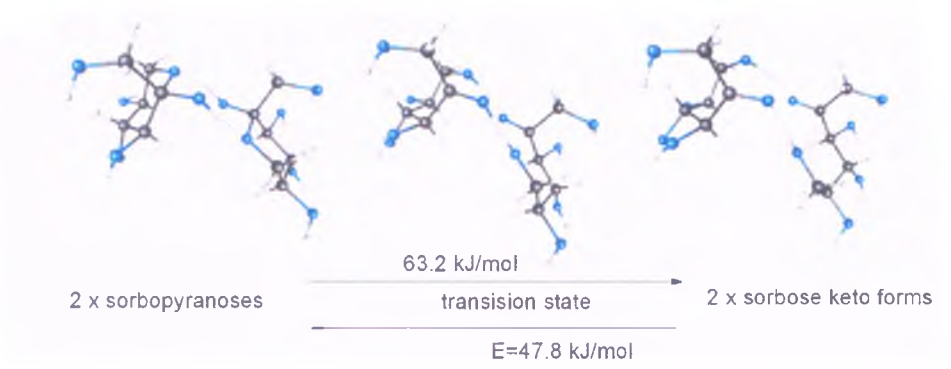


**Figure 3.9:** Visualization of double exchange mechanism calculated in $\alpha$-sorbopyranose

very close to the experimental one. As one cannot be certain, which elementary process is monitored by means of dielectric spectroscopy, more calculations in monosaccharides together with experimental studies have to be performed.

Similar result as for the L-sorbose was obtained for D-fructose. Formation of $\beta$-pyranoses in the mechanism of double proton exchange is connected with activation energy equal to 58.3 kJ/mol.

## 3.3 Mechanism of mutarotation

The studied monosaccharides exist as pure crystalline anomers. Crystalline L-sorbose is built of $\alpha$-pyranose, while D-ribose and D-fructose are built of $\beta$-pyranoses only. After melting, sample becomes liquid, thus the sugars start mutarotating. Melting temperature of monosaccharides is greater than 373 K and at such high temperature mutarotation occurs very quickly and, consequently pyranoses form an equilibrium almost instantly (from seconds to minutes). In the D-ribose and L-sorbose, probably about 10-15% of furanoses is created. In the D-fructose probably about 30% of furanoses is formed (population data are

from aqueous solution - not necessarily valid for anhydrous pure saccharides). When the saccharide is quenched to the near room temperatures, high temperature equilibrium becomes disturbed and new equilibration process starts. At low temperature equilibrium, population of the most stable pyranoses should be higher (lower temperature should favor more energetically stable tautomer) and, therefore transformation of furanoses into pyranose can be observed. In order to validate this theory, dipole moments analysis was performed in D-ribose and D-fructose. Static permittivity behavior in D-ribose and D-fructose is opposite. In the former saccharide it drops, while in the latter it rises. When one compares this to the calculations of dipole moments performed for D-ribose and D-fructose there is a striking connection. Pyranosidic ring of D-ribose has lower dipole moment than the furanoses, while in case of D-fructose pyranosidic ring has higher dipole moment than furanoses. Therefore, formation of $\beta$-pyranoses in both saccharides should change dielectric constant in the way that was described in the "static permittivity" section, i.e. in the opposite directions.

Sigmoidal shape of the kinetic curve at low temperature in D-fructose is an indication that the last of few consecutive reactions is monitored. Therefore, the obtained rate constants $k$ are probably related to the formation process of pyranoses ($\beta$ in case of fructose and ribose and $\alpha$ in case of sorbose).

The calculated energies of pyranose formation should be directly compared to activation energies obtained from dielectric measurements. Comparison of experimental and calculated activation energies can be found in Table 3.6. The results shown in Table 3.6 clearly indicate that in supercooled liquid phase, the mechanism based on external proton transfer dominates. The only molecules which can act as proton carrier are water ($H_2O$) and other monosaccharide unit (in

| | D-fructose | L-sorbose |
|---|---|---|
| Internal proton transfer | 165 kJ/mol | 138 kJ/mol |
| Water proton transfer | 66 kJ/mol | 76 kJ/mol |
| Saccharide proton transfer | 58 kJ/mol | 48 kJ/mol |
| Experimental value | 107 kJ/mol | 68 kJ/mol |

**Table 3.6:** Comparison of experimental value of activation energy with calculations accounted for most stable tautomer formation.

calculations, tautomer with highest population was used as a proton donor). The studied sugars were anhydrous, but extraordinary hygroscopic properties made it impossible to prepare totally dry sample. Therefore, it is reasonable to assume that small water amount can be enclosed in the sugar amorphous matrix. Activation energy in case of the mechanism with an additional water molecule is closest to the experimental result in L-sorbose. Small molecule of water is much more mobile than a saccharide molecule, and therefore if water is present in the system it can be involved in mutarotation mechanism. Energy of water diffusion in sugar amorphous matrix is about 60 kJ/mol (102) and above the sugar's glass transition temperature, mobility of water is higher than the speed of reaction. In case of saccharide-saccharide reaction structural relaxation is also faster than the speed of reaction (compare $1/k$ with $\tau_{max}$). Comparison of structural relaxation rate and mutaroation rate has been shown in Figure 3.10. As one can see, in the glassy state (about 10 K below $T_g$) mutarotation becomes faster than structural relaxation, thus the rate of mutarotation is controlled by diffusion in this system. Moreover, internal proton transfer in the glassy state, should dominate over the external one, as the latter is suppressed by high viscosity.

As the studied systems were pure sugars, the described mechanism of double

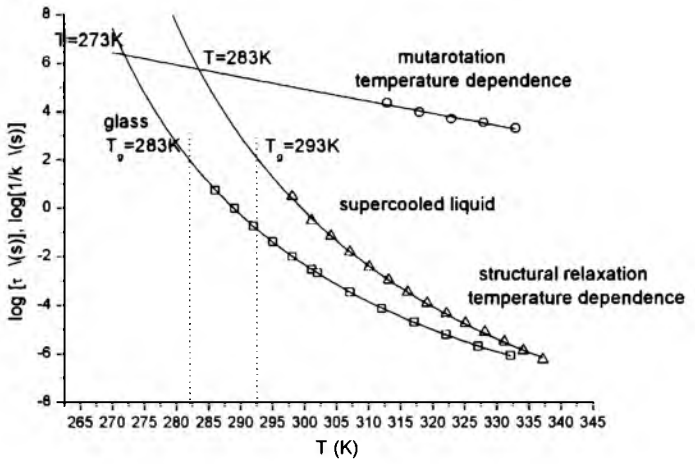


**Figure 3.10:** Crossover of curves describing structural relaxation and mutarotation behavior. Two different curves have been plotted for D-fructose structural relaxation. The left one is for the quenched sample (lower $T_g$) and the right one for equilibrated sample.

proton exchange between two saccharide units should be dominant above glass transition temperature (even when few percent of water has been absorbed from air). As one can see in Table 3.6, although activation energies of saccharide proton transfers are closest to the real system, there is a large difference. The values are about 40% lower than the experimental ones. However, the obtained activation energies can be slightly underestimated in most cases by means of DFT/B3LYP method. Moreover, since monosaccharides are very polar and hydrogen bonding systems, activation energies cannot be estimated with high accuracy without taking into account interaction with surroundings.

Due to the fact, that experimentally derived activation energy is much lower than the calculated energy for internal transfer and higher than the calculated energy for external proton transfer, there is a possibility that these two mechanisms occur simultaneously in the supercooled liquid phase. External proton

transfer is preferred due to the lower energy, however it is bimolecular reaction. Internal proton transfer is not preferred due to the energy but it is unimolecular reaction. As in a supercooled liquid state cooperative motion of molecules suffers due to the high viscosity, unimolecular reactions have an advantage in such environment. Therefore, experimental value of mutarotation can be ascribed to the mixed mechanism, in which internal and external proton transfers coexist. When the sample approaches glass transition, cooperative motion of molecules becomes so slow that internal transfer becomes dominant.

## 3.4 Summary

Performed experimental and theoretical studies have been used to formulate the conclusion, that in supercooled liquid state of saccharides, the mechanism of mutarotation is complex. Analysis of dipole moments lead to the conclusion that in supercooled liquid state formation stage of most stable tautomer i.e. $\beta$-pyranose in case of D-fructose and D-ribose and $\alpha$-pyranose in case of L-sorbose, was observed. Comparison of theoretical and experimental studies indicate, that both mechanisms of mutarotation (external and internal proton transfers) in supercooled liquid state can occur simultaneously. Two molecules were checked as proton carriers in the external type of mechanism: water and saccharide molecules. The activation energy in both cases, i.e. when proton is transfered by water or saccharide, is similar. The measured saccharides were anhydrous, thus water molecules can be present in the sample only as contaminants. Therefore, sugar - sugar proton exchange is more probable scenario for an external proton transfer.

An external proton transfer should be suppressed at low temperatures, when

sugar approaches glass transition, which is caused by the enormous viscosity. In the glassy state the internal proton transfer should start to dominate.

Mutarotation is connected with the dynamics of hydrogen bonds, as the secondary mode in dielectric spectrum is sensitive to this reaction. The secondary mode has different dielectric strength or relaxation time after equilibration period.

Dielectric spectroscopy has proved to be a great method for studying tautomerization reactions in supercooled liquid state. Other methods, such as PVT or refractive index measurements could be also useful in kinetic studies in viscous phases.

# 4

# Materials & methods

## 4.1 Theoretical calculations

Initial monosaccharide structures were modeled by hand in the ACD Chemsketch 12.0 and optimized by the molecular mechanics implemented in this package. Then, the structures were optimized on the B3LYP/6-31+G(d,p) level of theory in the Orca quantum package ver. 2.8 (103). Transition states were calculated in Orca 2.8. At the beginning, the relaxed geometry scan was performed. In case of internal proton transfer, the distance between oxygen in ring and hydrogen from anomeric hydroxyl group was changed during the scan. In case of an external proton transfer scan was more complicated. At the beginning, water or second saccharide molecule was placed in such a way that the hydrogen from water or hydrogen from anomeric hydroxyl group of second saccharide was close to the oxygen from the ring of the first saccharide. Distance between these atoms was set to the 1.15 Åand then the geometry scan with changing distance between water oxygen or second saccharide oxygen and hydrogen from anomeric hydroxyl group of first saccharide was made. Transition state optimization with preceding

calculations of full Hessian was then performed on the structure with the highest energy. The minima and transition states were checked by vibrational analysis. Molecules were visualized in gOpenMol 3.00 program (104, 105).

## 4.2 Studied samples

D-fructose, D-ribose and L-sorbose were bought at Sigma-Aldrich company. L-sorbose had > 98% purity, while D-ribose and D-fructose had > 99% purity. All these substances were crystalline. L-sorbose consisted of $\alpha$-pyranose tautomer, while D-ribose and D-fructose consisted of $\beta$-pyranose tautomers.

## 4.3 Experimental methods

### 4.3.1 Dielectric spectroscopy

Dielectric measurements were carried out by Novocontrol spectrometer (see Figure 4.1). The spectrometer measures the impedance of capacitor filled with dielectric material over a wide frequency range. Complex permittivity of dielectric material is evaluated from the impedance measurements. The whole measurement setup consists of:

- Alpha analyzer - which measures impedance in the frequency range from $10^{-3}$ to $10^{-6}$ Hz
- Sample cell - connects the sample capacitor to the impedance analyzer and mounts it into a cryostat for temperature control. Sample cell is shown in Figure 4.2

**Figure 4.1:** Broadband dielectric spectroscopy measurement setup.

- Temperature control system - which adjusts the sample capacitor to fixed temperatures or continuously changes temperature. Quattro system employed with a nitrogen gas cryostat was used.

- Computer with software for system control and evaluation - Hardware was controlled by WinDETA software. Curves from dielectric spectrum were fitted in WinFit software by Novocontrol

For dielectric measurements a capacitor built of two round plates ($\Phi$=20 mm) separated by a teflon spacer (0.1 mm) was used. The sample was placed in a capacitor, then it was heated to the melting point of studied saccharide, and after melting, the sample was quenched. Thereafter, the capacitor was placed in the sample cell and after the temperature stabilization time measurement was initiated. Dielectric spectrum was then analyzed by WinFit. Structural relaxation curves were fitted by the Havriliak-Negami function with an additional

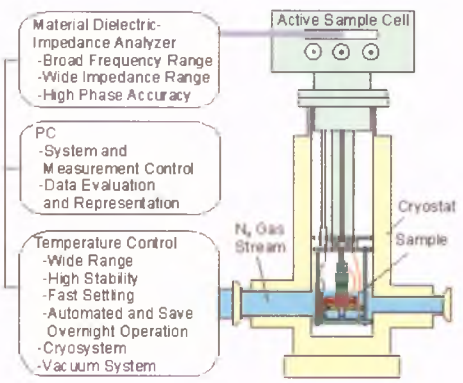


**Figure 4.2:** Sample cell

DC-conductivity term.

### 4.3.2 Refractive index

Refractive index was measured by means of Abbe's refractometer. Temperature was stabilized by water ultra-thermostat. The melted and warm sugar was poured onto prism and time measurement was carried out. Sodium lamp was used as a light source.

# References


[1] A. Wiśniewski and J. Madaj, *Podstawy Chemii Cukrów*, Argra-Envirolab 1997, Poznań-Gdańsk, 1997. 1

[2] A. Zejc and M. Gorczyca, *Chemia leków*, PZWL, Warszawa, 1998.

[3] P. M. Collins and R. J. Ferrier, *Monosacharides, Their Chemistry and Their Roles in Natural Products*, J. Wiley & Sons, Chichester, New York, Brisbane, Toronto, Singapore, 1995.

[4] A. Cziczibabin, *Podstawy Chemii Organicznej*, PWN, Warszawa, 1961.

[5] Z. Györgydéak and I. Pelyvas, *Monosaccharide Sugars*, Academic Press, San Diego, 1997.

[6] T. T. Kozlowski and S. G. Pallardy, *Physiology of Woody Plants*, Academic Press, San Diego, 1996.

[7] P. Kubikowski and W. Kostowski, editors, *Farmakologia, podstawy farmakoterapii*, PZWL, Warszawa, 1979.

[8] C. Nanitescu, *Chemia organiczna*, PWN, Warszawa, 1969.

[9] E. Pawełczyk, editor, *Chemia leków*, PZWL, Warszawa, 1996.

[10] G. L. Patrick, *Chemia medyczna*, WNT, Warszawa, 2003.

[11] W. Pigman and D. Horton, editors, *The Carbohydrates, Chemistry/Biochemistry*, Academic Press, New York and London, 1970.

[12] E. Pijanowski, M. Dłużewski, A. Dłużewska, and A. Jarczyk, *Ogólna technologia żywności*, WNT, Warszawa, 1996.

[13] D. E. Levy and P. Fugedi, editors, *The Organic Chemistry of Sugars*, CRC Press Taylor and Francis Group, US, 2006.

[14] J. F. Robyt, *Essentials of Carbohydrate Chemistry*, Springer-Verlag New York, Inc., 1998.

[15] C. Ratledge and B. Kristiansen, editors, *Basic Biotechnology*, Cambridge University Press, Cambridge, 2001.

[16] J. Rawn, *Biochemistry*, Beil Patterson Pub., North Carolina, 1989.

[17] Z. E. Sikorski, editor, *Chemia żywności. Skład, przemiany i własności żywności*, WNT, Warszawa, 2000.

[18] W. Steglich, B. Fugmann, and S. Lang-Fugmann, editors, *Natural Products Rompp Encyklopedia*, Georg Thieme Verlag, Stuttgard, New York, 2000.

[19] L. Stryer, *Biochemia*, WN PWN, Warszawa, 2003.

[20] H. Walter, *Polysaccharide Dispersions*, Academic Press, San Diego, 1997.

[21] F. Świderski, editor, *Żywność wygodna i żywność funkcjonalna*, WNT, Warszawa, 1999.

[22] A. Kołodziejczyk, *Naturalne związki organiczne*, PWN, Warszawa, 2006. 1

[23] M. Cox and D. Nelson, *Lehninger Principles of Biochemistry*, W. H. Freeman, New York, 4th edition, 2005. 2

[24] K. N. Kirschner and R. J. Woods, *Proc. Natl. Acad. Sci. U.S.A.* **98**, 10541 (2001). 3

[25] T. V. Chalikian, *J. Phys. Chem. B* **102**, 6921 (1998).

[26] V. Molinero and W. A. Goddard, *Phys. Rev. Lett.* **95**, 045701 (2005).

[27] H. Weingartner, A. Knocks, S. Boresch, P. Hochtl, and O. Steinhauser, *J. Chem. Phys.* **115**, 1463 (2001).

[28] V. H. Tran and J. W. Brady, *Biopolymers* **29**, 961 (2004).

[29] J. N. Reitter, R. E. Means, and R. C. Desrosiers, *Nature Medicine* **4**, 679 (1998).

[30] T. R. Noel, S. G. Ring, and M. A. Whittam, *J. Phys. Chem.* **96**, 5662 (1992).

[31] Gangasharan and S. S. N. Murthy, *J. Chem. Phys.* **99**, 9865 (1993).

[32] M. Tyagi and S. Murthy, *Carbohydr. Res.* **341**, 650 (2006).

[33] D. Champion, M. Maglione, G. Niquet, D. Simatos, and M. L. Meste, *J. Therm. Anal. Calorim.* **71**, 249 (2003).

[34] D. Meiner, J. Einfeldt, and A. Kwasniewski, *J. Non-Cryst. Solids* **275**, 199 (2000).

[35] T. R. Noel, R. Parker, and S. G. Ring, *Carbohydr. Res.* **282**, 193 (1996).

[36] A. Faivre, G. Niquet, M. Maglione, J. Fornazero, J. F. Jal, and L. David, *Eur. Phys. J. B* **10**, 277 (1999).

[37] T. R. Noel, R. Parker, and S. G. Ring, *Carbohydr. Res.* **329**, 839 (2000).

[38] A. M. Wachner and K. R. Jeffrey, *J. Chem. Phys.* **111**, 10611 (1999).

[39] Gangasharan and S. S. N. Murthy, *J. Phys. Chem.* **99**, 12349 (1995).

[40] A. D. Gusseme, L. Carpentier, J. F. Willart, and M. Descamps, *J. Phys. Chem. B* **107**, 10879 (2003).

[41] L. Finegold, F. Franks, and R. H. M. Haltey, *J. Chem. Soc., Faraday Trans. 1* **85**, 2945 (1989).

[42] D. I. Freedberg, *J. Amer. Chem. Soc.* **124**, 2358 (2002).

[43] L. Poppe and H. V. Halbeek, *J. Amer. Chem. Soc.* **114**, 1092 (1992).

[44] C. Baraguey, D. Mertens, and A. Dolle, *J. Phys. Chem. B* **106**, 6331 (2002).

[45] D. van Dusschoten, U. Tracht, A. Heuer, and H. W. Spiess, *J. Phys. Chem. A* **103**, 8359 (1999).

[46] G. R. Moran, K. R. Jeffrey, J. M. Thomas, and J. R. Stevens, *Carbohydr. Res.* **328**, 573 (2000). 3

[47] A. P. Dubrunfaut, *Compt. Rend.* **23**, 38 (1846). 9

[48] C. S. Hudson, *J. Am. Chem. Soc.* **32**, 889 (1910). 9

[49] F. V. Sander, *J. Biol. Chem.* **148**, 311 (1943). 10

[50] R. Behrends and U. Kaatze, *Biophys. Chem.* **111**, 89 (2004).

[51] N. L. Barc'H, J. M. Grossel, P. Looten, and M. Mathlouthi, *Food Chem.* **74**, 119 (2001).

[52] A. E. Flood, M. R. Johns, and E. T. White, *Carboh. Res.* **288**, 45 (1996). 10, 18

[53] P. Wlodarczyk, K. Kaminski, M. Paluch, and J. Ziolo, *J. Phys. Chem. B* **113**, 4379 (2009). 11, 47

[54] P. Wlodarczyk, K. Kaminski, M. Dulski, S. Haracz, M. Paluch, and J. Ziolo, *J. Non-Cryst. Solids* **356**, 738 (2010).

[55] P. Wlodarczyk, K. Kaminski, S. Haracz, M. Dulski, M. Paluch, J. Ziolo, and M. Wygledowska-Kania, *J. Chem. Phys.* **132**, 195104 (2010).

[56] P. Wlodarczyk, M. Paluch, L. Hawelek, K. Kaminski, and J. Pionteck, *J. Chem. Phys.* **134**, 175102 (2011). 47

[57] N. Dujardin, E. Dudognon, J.-F. Willart, A. Hédoux, Y. Guinet, L. Paccou, and M. Descamps, *J. Phys. Chem. B* **115**, 1698 (2011). 47

[58] N. Dujardin, J. F. Willart, E. Dudognon, A. Hedoux, Y. Guinet, L. Paccou, B. Chazallon, and M. Descamps, *Solid State Commun.* **148**, 78 (2008). 11, 58

[59] A. Broido, Y. Houminer, and S. P. and, *J. Chem. Soc. B* **5**, 411 (1966). 11, 65

[60] R. S. Shallenberger, *Sugar Structure and Taste*, chapter 16, pp. 256–263. 13

[61] J. G. Gurney, J. M. Pogoda, E. A. Holly, S. S. Hecht, and S. Preston-Martin, *Journal of the National Cancer Institute* **89**, 1072 (1997). 13

[62] R. J. Johnson, M. S. Segal, Y. Sautin, T. Nakagawa, D. I. Feig, D. Kang, M. S. Gersch, S. Benner, and L. G. Sánchez-Lozada, *Am. J. Clin. Nutr.* **86**, 899 (2007). 18

[63] S. S. Elliott, N. L. Keim, J. S. Stern, K. Teff, and P. J. Havel, *Am. J. Clin. Nutr.* **76**, 911 (2002).

[64] M. Tordoff and A. Alleva, *Am. J. Clin. Nutr.* **51**, 963 (1990).

[65] G. A. Bray, S. J. Nielsen, and B. M. Popkin, *Am. J. Clin. Nutr.* **79**, 537 (2004). 18

[66] Y. Hellsten, L. Skadgauge, and J. Bangsbo, *Am. J. Physiol.* **286**, R182 (2004). 19

[67] P. C. Tullson and R. L. Terjung, *Am. J. Physiol.* **261**, C342 (1991). 20

[68] W. Koch and M. C. Holthausen, *A Chemist's guide to density functional theory*, Wiley-VCH Verlag, Weinheim, New York, Chichester, Brisbane, Singapore, Toronto, 2001. 20

[69] L. Piela, *Idee chemii kwantowej*, PWN, Warszawa, 2003. 20

[70] J. P. Perdew and S. Kurth, *1. Density functionals for non-relativistic Coulomb Systems in the new century*, volume 620 of *Lecture Notes in Physics*, Springer Verlag, Berlin, 2003. 22

[71] S. Ye and F. Neese, *Inorg. Chem.* **49**, 772 (2010). 23

[72] S. Kossmann and F. Neese, *J. Chem. Theo. Comp.* **6**, 2325 (2010).

[73] S. Grimme and F. Neese, *J. Chem. Phys.* **127**, 154116 (2007).

[74] F. Neese, T. Schwabe, and S. Grimme, *J. Chem. Phys.* **126**, 124115 (2007).

[75] S. Kossmannn, B. Kirchner, and F. Neese, *Molec. Phys.* **105**, 2049 (2007). 23

[76] A. D. Becke, *J. Chem. Phys.* **98**, 1372 (1993). 24

[77] C. Lee, W. Yang, and R. G. Parr, *Phys. Rev. B* **37**, 785 (1988).

[78] S. H. Vosko, L. Wilk, and M. Nusair, *Can. J. Phys.* **58**, 1200 (1980).

[79] P. J. Stephens, F. J. Devlin, C. F. Chabalowski, and M. J. Frisch, *J. Phys. Chem.* **98**, 11623 (1994). 24

[80] R. A. Marcus and O. K. Rice, *J. Phys. Colloid Chem.* **55**, 894 (1951). 35

[81] R. A. Marcus, *J. Chem. Phys.* **20**, 359 (1952). 35

[82] H. Eyring, *Journal of Chemical Physics* **3**, 107 (1935). 35

[83] H. M. Rosentock, M. B. Wallenstein, A. L. Waihhaftig, and H. Eyring, *Proc. Natl. Acad. Sci. U.S.A.* **38**, 667 (1952).

[84] J. C. Giddincs and H. Eyring, *J. Chem. Phys.* **22**, 538 (1954). 35

[85] J. L. Magee, *Proc. Natl. Acad. Sci. U.S.A.* **38**, 764 (1952). 35

[86] B. S. Rabinovitch and D. W. Setser, *AdV. Photochem.* **3**, 1 (1964). 35

[87] D. L. Bunker, *J. Chem. Phys.* **37**, 393 (1962). 35

[88] D. L. Bunker, *J. Chem. Phys.* **40**, 1946 (1964).

[89] D. L. Bunker and M. Pattengill, *J. Chem. Phys.* **48**, 772 (1968).

[90] D. L. Bunker and W. L. Hase, *J. Chem. Phys.* **59**, 4621 (1973). 35

[91] E. Tombari, G. Salvetti, C. Ferrari, and G. P. Johari, *J. Phys. Chem. B* **108**, 16877 (2004). 47

[92] E. Tombari, C. Cardelli, G. Salvetti, and G. P. Johari, *J. Mol. Struct.* **559**, 245 (2001). 47

[93] J. Fan and C. A. Angell, *Termochim. Acta* **280–281**, 523 (1996). 47

[94] R. Lefort, V. Caron, J.-F. Willart, and M. Descamps, *Solid State Comm.* **149**, 329 (2006). 47

[95] L. P. Singh, A. A. a, and J. Colmenero, *Carbohydr. Res.* **346**, 2165 (2011). 47, 56

[96] K. Kaminski, E. Kaminska, M. Paluch, J. Ziolo, and K. L. Ngai, *J. Phys. Chem. B* **110**, 25045 (2006). 49

[97] K. Kaminski, P. Wlodarczyk, K. Adrjanowicz, E. Kaminska, Z. Wojnarowska, and M. Paluch, *J. Phys. Chem. B* **114**, 11272 (2010). 49, 56

[98] N. L. Barc'H, J. M. Grossel, P. Looten, and M. Mathlouthi, *Food Chem.* **74**, 119 (2001). 58

[99] G. de Wit, A. P. G. Kieboom, and H. van Bekkum, *Recl. Trav. Chim. Pays-Bas* **98**, 355361 (1979).

[100] H. Friebolin, M. Supp, R. Brossmer, G. Keilich, and D. Ziegler, *Angew. Chem. Int. Ed. Engl.* **19**, 208 (1980). 58

[101] Z. Wojnarowska, P. Wlodarczyk, K. Kaminski, K. Grzybowska, L. Hawelek, and M. Paluch, *J. Chem. Phys* **133**, 094507 (2010). 58

[102] R. H. Tromp, R. Parker, and S. G. Ring, *Carboh. Res.* **303**, 199 (1997). 68

[103] F. Neese, Orca - an ab initio, Density Functional and Semiempirical program package, Version 2.6, University of Bonn 2008. 72

[104] L. Laaksonen, *J. Mol. Graph.* **10**, 33 (1992). 73

[105] D. L. Bergman, L. Laaksonen, and A. Laaksonen, *J. Mol. Graph. Model.* **15**, 301 (1997). 73

# Declaration

I herewith declare that I have produced this paper without the prohibited assistance of third parties and without making use of aids other than those specified; notions taken over directly or indirectly from other sources have been identified as such. This paper has not previously been presented in identical or similar form to any other Polish or foreign examination board.

The thesis work was conducted from 2009 to 2012 under the supervision of prof. Marian Paluch at Institute of Physics, University of Silesia in Katowice.

Katowice, 31-05-2012